

Generalized Couette–Poiseuille flow with boundary mass transfer

By F. MARQUES¹, J. SANCHEZ¹ AND P. D. WEIDMAN²

¹Departamento Física Aplicada, Universitat Politècnica de Catalunya, Jordi Girona Salgado s/n, Mòdul B4 Campus Nord, 08034 Barcelona, Spain

²Department of Mechanical Engineering, University of Colorado, Campus Box 427, Boulder, CO 80309-0427, USA.

(Received 26 December 1996 and in revised form 10 June 1998)

A generalized similarity formulation extending the work of Terrill (1967) for Couette–Poiseuille flow in the annulus between concentric cylinders of infinite extent is given. Boundary conditions compatible with the formulation allow a study of the effects of inner and outer cylinder transpiration, rotation, translation, stretching and twisting, in addition to that of an externally imposed constant axial pressure gradient. The problem is governed by η , the ratio of inner to outer radii, a Poiseuille number, and nine Reynolds numbers. Single-cylinder and planar problems can be recovered in the limits $\eta \rightarrow 0$ and $\eta \rightarrow 1$, respectively. Two coupled primary nonlinear equations govern the meridional motion generated by uniform mass flux through the porous walls and the azimuthal motion generated by torsional movement of the cylinders; subsidiary equations linearly slaved to the primary flow govern the effects of cylinder translation, cylinder rotation, and an external pressure gradient. Steady solutions of the primary equations for uniform source/sink flow of strength F through the inner cylinder are reported for $0 \leq \eta \leq 1$. Asymptotic results corroborating the numerical solutions are found in different limiting cases. For $F < 0$ fluid emitted through the inner cylinder fills the gap and flows uniaxially down the annulus; an asymptotic analysis leads to a scaling that removes the effect of η in the pressure parameter β , namely $\beta = \pi^2 R^{*2}$, where $R^* = F(1 - \eta)/(1 + \eta)$. The case of sink flow for $F > 0$ is more complex in that unique solutions are found at low Reynolds numbers, a region of triple solutions exists at moderate Reynolds numbers, and a two-cell solution prevails at large Reynolds numbers. The subsidiary linear equations are solved at $\eta = 0.5$ to exhibit the effects of cylinder translation, rotation, and an axial pressure gradient on the source/sink flows.

1. Introduction

A generalized similarity formulation is presented for steady swirling Couette–Poiseuille flow in an annulus of infinite axial extent. Building on the work of Terrill (1967), we have included all external forcings admitted by the similarity *ansatz* that produce motion in the annulus. These forcings fall into three separate categories as described below. Since the pioneering work of Berman (1953), a number of papers investigating the flow generated by uniform wall transpiration in planar, cylindrical, and annular geometries have appeared. References to major works in this category (I) of flows and to papers dealing with their stability may be found in Brady (1984) and Durlinsky & Brady (1984). In a second category (II) are flows generated by

moving walls. Here, of course, a plethora of work is available on the stability of circular Couette flow and the reader is referred to a comprehensive literature review by Tagg (1994). Included in this category are flows driven by the spiralling motion of a cylinder wall as in the experimental study by Ludweig (1964) and in the stability analysis of Ali & Weidman (1993). Yet another example of boundary-driven flows are those produced by extensional wall motion as reported by Brady & Acrivos (1981) and Durlofsky & Brady (1984). The third and final category (III) of flows admitted by the similarity formulation are Poiseuille flows in planar, circular, and annular geometries.

Part of the motivation for the present investigation stems from an interest in determining steady solutions that mimic the flow in a rotating membrane separator. In this system a filtrate enters one end of the annulus between a stationary outer cylinder and a porous inner cylinder, and as the mixture flows axially, filtrate passes through the filter into the inner cylinder leaving the concentrate in the annular gap; in this manner the filtrate is collected from within the inner cylinder and the concentrate is collected at the downstream end of the annulus. Rotation applied to the inner cylinder sustains a high shear across the gap that serves to reduce concentrate 'caking' on the surface of the filter. These dynamic filtration devices are currently in use for the separation of plasma from whole blood (Gilcher 1986), for the separation and concentration of other biologic suspensions (Hildebrandt & Saxton 1987) and, in its original form, for the separation of milk (Hallstrom & Lopez-Leiva 1978). Further details concerning rotating membrane separators and their applications may be found in the review article by Lueptow (1995).

Although the underlying physics of the operation of these filters is poorly understood, it is clear that the flow in the gap is driven by mechanisms from the three categories described above, namely (I) suction through the inner cylinder, (II) rotation of the inner cylinder, and (III) an axial pressure gradient. Flows produced by multiple driving forces have been studied in the past. For example, Takeuchi & Jankowski (1981) reported on the stability of circular Couette flow (II) with an axial throughflow (III). Min & Lueptow (1994) reported on the stability of circular Couette flow (II) with radial throughflow across the annular gap which is a degenerate case of (I). Zaturka & Banks (1995) studied the stability of pipe flow driven by the combined effects of wall suction (I) and wall acceleration (II). Very recently Johnson & Lueptow (1997) have reported an analysis of the flow between porous (I) rotating (II) cylinders with an axial pressure gradient (III) that appears to be the first investigation of the stability of a base flow generated by mechanisms from all three categories.

It is understood that similarity formulations often lead to regions of no solution or regions of multiple solutions, both signalling the breakdown of the similarity method that often can be resolved by a finite length cylinder analysis. This is especially true in suction flows where entrance effects penetrate long distances from the entrance region. A case in point is porous tube flow driven by uniform suction. Weissberg (1959) made an analysis of inlet flow development for this problem using an integral method and concluded that the suction solutions cannot evolve into the (infinite cylinder) self-similar flow for Reynolds numbers Re exceeding 2.3, approximately. Brady (1984) performed a detailed analysis for suction flow development in uniformly porous ducts, verifying the conjecture by Weissberg (1959) for cylinders and further showing that channel flows exhibit non-similar solutions above a Reynolds number $Re \simeq 6$, in spite of the fact that self-similar solutions are available for all positive and negative Reynolds numbers. These entrance effects are likely to be important in a rotating membrane separator at high Reynolds numbers.

Keeping in mind the finite cylinder length problems noted above and other limitations of self-similar solutions discussed by Barenblatt (1996), we present in §2 a generalized similarity formulation that depends on eleven independent parameters and outline the numerical solution procedure. Low-Reynolds-number expansions for pure suction/blowing through an inner porous wall are given in §3. Numerical solutions extending these results to high blowing Reynolds numbers and an approximate asymptotic analysis are given in §4. Also in §4 some effects of inner and outer cylinder rotation, of cylinder translation, and of an axial pressure gradient on the source flow at the fixed radius ratio $\eta = 0.5$ are elucidated. In §5 the same ground is covered as in §4, but for sink flow through the inner cylinder. A discussion of results and concluding remarks are given in §6.

2. Mathematical formulation

We consider infinitely long cylinders of inner radius r_i^* and outer radius r_o^* . The gap between the cylinders is $d = r_o^* - r_i^*$. Assuming incompressible flow and constant kinematic viscosity ν , all variables may be rendered dimensionless using $d, d^2/\nu, \nu^2/d^2$ as units for space, time, and the reduced pressure (p^*/ρ). Let (u, v, w) be the velocity components along cylindrical coordinate directions (r, θ, z) , respectively. We seek only steady axisymmetric solutions. With flow through the porous boundaries, a net axial volume flux is generated, and hence the velocity and pressure fields must depend on the axial coordinate. Some assumption on that z -dependence has to be made. When the radial velocity $u(r, z)$ is a z -polynomial of degree N with coefficient functions of r , the Navier–Stokes equations require that v, w and p be z -polynomials of degree $N + 1, N + 1,$ and $2N + 2,$ respectively, in which case $7N + 8$ equations for $5N + 8$ unknown radial functions are obtained. Thus $N = 0$ for similarity and the primitive variables must take the form

$$u(r), \quad v(r, z) = v_0(r) + zv_1(r), \quad w(r, z) = w_0(r) + zw_1(r), \quad p(r, z). \quad (2.1)$$

The equation of continuity is satisfied by $u(r) = f(r)/r$ and $w_1 = -f'(r)/r$ in which case the Navier–Stokes equations yield

$$D \left[D_+ D \frac{f'}{r} + \left(\frac{f'}{r} \right)^2 - \frac{f}{r} D \frac{f'}{r} \right] = -\frac{2}{r} v_1^2, \quad (2.2)$$

$$D D_+ v_0 - \frac{f}{r} D_+ v_0 = w_0 v_1, \quad (2.3)$$

$$D D_+ v_1 - \frac{f}{r} D_+ v_1 + \frac{f'}{r} v_1 = 0, \quad (2.4)$$

$$D \left[D_+ D w_0 + \frac{1}{r} (f' w_0 - f w_0') \right] = \frac{2}{r} v_0 v_1, \quad (2.5)$$

where $D = \partial_r$ and $D_+ = D + 1/r$. The most general boundary conditions corresponding to (2.1) are obtained by assigning arbitrary values to $f, f', v_0, v_1,$ and w_0 on the cylinder walls. The values of f give uniform radial flows through each cylinder, while those for v_0 and w_0 correspond to uniform rotation and axial translation of the cylinders, respectively. Taking into account the Galilean invariance of the problem, the axial motion of both cylinders can be reduced to the case where only the inner cylinder translates, and hence we set $w_0(r_o) = 0$ without loss of generality. The values of f' and v_1 give extensional and torsional motion to the walls with axial and azimuthal velocities linearly increasing with z , features that apparently are not realistic even for

an elastic cylinder. The real motivation for these boundary conditions comes from two-fluid problems, to which the present formulation also applies, with appropriate interfacial boundary conditions. For example, Brady & Acrivos (1981) were led to consider the self-similar flow driven by an accelerating surface velocity as a result of studying the flow induced in a long slender drop of one fluid placed in the extensional flow of a second, immiscible fluid.

In dimensional variables, denoted by an asterisk, the boundary conditions for the general flow described above are given by

$$u^*(r_i^*) = U_i, \quad u^*(r_o^*) = U_o, \quad (2.6)$$

$$v^*(r_i^*, z^*) = r_i^* \Omega_i + z^* \tau_i, \quad v^*(r_o^*, z^*) = r_o^* \Omega_o + z^* \tau_o, \quad (2.7)$$

$$w^*(r_i^*, z^*) = W + z^* \gamma_i, \quad w^*(r_o^*, z^*) = z^* \gamma_o, \quad (2.8)$$

where Ω_i and Ω_o are the angular velocities of the cylinders, W is the translation speed of the inner cylinder, and U_i and U_o are the uniform suction velocities through the porous cylinder walls. We have also introduced γ and τ for the extensional and torsional cylinder wall strain rates, respectively.

The independent dimensionless parameters appearing in this problem are: the radius ratio $\eta = r_i^*/r_o^*$ which fixes the geometry of the annulus; the rotational Reynolds numbers $R_i = dr_i^* \Omega_i / \nu$ and $R_o = dr_o^* \Omega_o / \nu$ of the inner and outer cylinders; the axial Reynolds number $R_a = dW / \nu$ measuring the translational velocity of the inner cylinder; the transpiration Reynolds numbers $F_i = r_i^* U_i / \nu$ and $F_o = r_o^* U_o / \nu$ proportional to the radial flux per unit axial length through each cylinder wall. Finally, we have the extensional Reynolds numbers $E_i = dr_i^* \gamma_i / \nu$ and $E_o = dr_o^* \gamma_o / \nu$, analogous to the shear Reynolds number introduced by Brady & Acrivos (1981), and the torsional Reynolds numbers $T_i = d^2 \tau_i / \nu$ and $T_o = d^2 \tau_o / \nu$ for each cylinder. The non-dimensional form of boundary conditions (2.6)–(2.8) is

$$f(r_i) = -F_i, \quad f(r_o) = F_o, \quad f'(r_i) = -E_i, \quad f'(r_o) = -E_o, \quad (2.9)$$

$$v_0(r_i) = R_i, \quad v_0(r_o) = R_o, \quad (2.10)$$

$$v_1(r_i) = T_i, \quad v_1(r_o) = T_o, \quad (2.11)$$

$$w_0(r_i) = R_a, \quad w_0(r_o) = 0. \quad (2.12)$$

Equations (2.2)–(2.4) were also obtained by Terrill (1967), although he considered only the case $R_i = R_o = R_a = E_i = E_o = T_i = T_o = 0$ and took $w_0 = v_0 = v_1 = 0$. Equation (2.5) for w_0 is third order in r , and we have only the two boundary conditions given in (2.12). This incompatibility is related to the invariance of the equations under the z -translation $z \rightarrow z - a$ which induces a shift in v_0 and w_0 given by

$$v_0 \rightarrow v_0 - av_1, \quad w_0 \rightarrow w_0 + af'/r \quad (2.13)$$

as can be seen from (2.1). Boundary conditions (2.10) and (2.12) change according to (2.13) and this degree of freedom may be resolved by examining the pressure. A straightforward but lengthy calculation gives

$$p(r, z) = \frac{f'}{r} - \frac{f^2}{2r^2} + \int_{\bar{r}}^r \frac{v^2}{r} dr + \alpha z - \frac{1}{2} \beta z^2 + p_0, \quad (2.14)$$

$$\alpha = \left[D_+ D w_0 + \frac{1}{r} (f' w_0 - f w_0') \right]_{r=\bar{r}}, \quad (2.15)$$

$$\beta = \left[D_+ D \frac{f'}{r} + \left(\frac{f'}{r} \right)^2 - \frac{f}{r} D \frac{f'}{r} \right]_{r=\bar{r}}, \quad (2.16)$$

where \bar{r} is an arbitrary radius in the fluid, and different choices only redefine the constant reference pressure p_0 . It is clear from (2.14) and (2.15) that α is the external axial pressure gradient $(dp/dz)_0$ uniquely associated with the axial flow w_0 . We fix the degree of freedom associated with the translational invariance by taking $\alpha = P$, where $P = d^3(dp^*/dz^*)_0/\rho v^2$ is the Poiseuille number. Then (2.15) with $\alpha = P$ is the remaining boundary condition for equations (2.2)–(2.5).

Equations (2.2) and (2.4) form a coupled system for f and v_1 . Equations (2.3) and (2.5) comprise a subsidiary linear system for v_0 and w_0 slaved to f and v_1 . The family of exact Navier–Stokes solutions then depends on eleven arbitrary parameters: the radius ratio, the nine Reynolds numbers, and the Poiseuille number.

2.1. Particular cases

In the particular case $T_i = T_o = 0, v_1 = 0$, the system of governing equations simplifies to

$$D_+D \frac{f'}{r} + \left(\frac{f'}{r}\right)^2 - \frac{f}{r}D \frac{f'}{r} = \beta, \quad f(r_i) = -F_i, \quad f(r_o) = F_o, \quad f'(r_i) = -E_i, \quad f'(r_o) = -E_o, \tag{2.17}$$

$$DD_+v - \frac{f}{r}D_+v = 0, \quad v(r_i) = R_i, \quad v(r_o) = R_o, \tag{2.18}$$

$$D_+Dw_0 + \frac{1}{r}(f'w_0 - fw'_0) = P, \quad w_0(r_i) = R_a, \quad w_0(r_o) = 0. \tag{2.19}$$

The constant β giving the quadratic z -dependence of the pressure enters in the third-order equation for f and must be determined in the course of solution using the four boundary conditions in (2.17). The velocity components v and w_0 are then obtained through solution of the slaved equations (2.18) and (2.19). The remaining velocity components are given by $u = f/r, w_1 = -f'/r$ and the pressure is obtained from (2.14) with $\alpha = P$.

Some well known solutions of (2.17) are obtained for special parameter values. When $F_i = F_o = E_i = E_o = 0$, then $f = \beta = 0$ and the analytic Couette–Poiseuille solution (cf. Joseph 1977) emerges:

$$u = 0, \quad v = Ar + \frac{B}{r}, \quad w = \frac{1}{4}P(r^2 - r_o^2) + C \log \frac{r}{r_o}, \quad p = \int^r \frac{v^2}{r} dr, \tag{2.20}$$

$$A = \frac{r_o R_o - r_i R_i}{r_o^2 - r_i^2}, \quad B = \frac{r_i r_o (r_o R_i - r_i R_o)}{r_o^2 - r_i^2}, \quad C = \frac{(r_o^2 - r_i^2)P + 4R_a}{4 \log(r_i/r_o)}. \tag{2.21}$$

When the radial mass fluxes through the porous walls are non-zero but equal, $-F_i = F_o = F \neq 0$ and $E_i = E_o = T_i = T_o = 0$, then $f = F$ and $\beta = 0$ and the explicit solution reported by Berman (1958) is found. If $P = R_a = T_i = T_o = 0$ the system is invariant under the mirror symmetry $z \rightarrow -z, (u, v, w) \rightarrow (u, v, -w)$ and therefore the solutions come in pairs which differ only in the sign of v_1 and w_0 . Also, for a given f , the equations for v_1 and w_0 are linear and homogeneous, and therefore $v_1 = w_0 = 0$, except for special forms of f allowing the existence of eigensolutions.

The general equations describing self-similar flows are not restricted to the flow in an annulus. In the limit $r_o \rightarrow \infty$ the similarity formulation for an external radial stagnation flow impinging on stationary cylinder (Wang 1974) or on a rotating cylinder with transpiration through the porous cylinder wall (Cunning, Weidman & Davis 1998) are obtained. The limit $r_i \rightarrow 0$ corresponds to the classical Poiseuille problem, but with swirl, in a rotating, linearly stretching and twisting porous pipe.

In the $r_i \rightarrow 0$ limit, one may also consider the viscous motion produced by a line source and/or a line vortex coincident with the axis of the cylinder. When $r_o \rightarrow \infty$ and $r_i \rightarrow 0$ simultaneously, the equations describing the viscous axisymmetric Burgers (1948) vortex (see Saffman 1992 for an excellent discussion of Burgers' vortices) in an unbounded fluid domain are recovered. The narrow gap limit $\eta \rightarrow 1$ includes plane Poiseuille, plane Couette, and Hiemenz stagnation-point flows, among others. Some of the limiting cases discussed above will be considered in §§3 and 4.

2.2. Numerical method

When F_i and F_o are arbitrary, the solution must be computed numerically. In what follows we consider the case $F_o = E_i = E_o = T_i = T_o = 0$ and $F_i = F$ corresponding to radial blowing/suction through the inner cylinder with an impermeable outer cylinder. Equation (2.17) for $f(r)$ is independent of R_i , R_o , R_a and P , and will be analysed in detail. Rotation, translation, and imposed axial pressure gradients modify the azimuthal and axial velocities determined from f , but not the radial velocity $u = f(r)/r$, and will be discussed later.

Owing to the boundary conditions in (2.17), it is not possible to convert this system to an initial-value problem as was done by Brady & Acrivos (1981) for the extensional wall problem. We find it convenient to obtain solutions using a Chebyshev-collocation technique outlined in Canuto *et al.* (1987).

Let h be the third-degree polynomial satisfying the four boundary conditions on f . Then f may be written in the form

$$f(r) = h(r) + (r_i - r)^2(r_o - r)^2 \sum_{n=0}^{N-2} f_n T_n[2(r - r_i) - 1], \quad (2.22)$$

where the T_n are Chebyshev polynomials of degree n , and f_n are the coefficients of a truncated series for $(f - h)/(r_i - r)^2(r_o - r)^2$ in terms of Chebyshev polynomials.

The approximations to f and β have been obtained by applying a continuation procedure due to Keller (1977) and Simó (1990) that allows the study of the dependence of solutions on system parameters. From the N coefficients f_n and from β the expression

$$G(f, \beta)_k = [D_+ D(f'/r) - f/r D(f'/r) + (f'/r)^2 - \beta](r_k) \quad (2.23)$$

is evaluated on a mesh of Gauss-Lobatto points $r_k = r_i + [1 + \cos(\pi(N-k)/N)]/2$, $k = 0, \dots, N-1$ chosen because they accumulate at the ends of the interval $[r_i, r_o]$ where boundary layers develop at large Reynolds number.

If the rank of $DG(f, \beta)$ is N , the nonlinear system (2.23) defines locally a curve of solutions depending on F which is followed using the continuation procedure. Solutions are moved away from $F = 0$ where $f = \beta = 0$ using the Stokes flow solution reported in §3. The solutions are extended to large values of F where the equations become increasingly stiff owing to the development of thin boundary layers at the cylinder walls.

In what follows β will be called the pressure gradient parameter. Other parameters of interest are the z -dependent wall shear stresses given by

$$\tau_{rz}(r_i) = -zf''(r_i)/r_i^2 = z\Sigma_i, \quad -\tau_{rz}(r_o) = zf''(r_o)/r_o^2 = z\Sigma_o, \quad (2.24)$$

in which we have used the fact that f' is zero on both cylinder walls. The constants Σ_i , Σ_o denote the inner and outer shear stress parameters, respectively.

In order to plot the streamlines for pure blowing and suction, observe that $\chi(r, z) = zf(r) - \int rw_o(r) dr$ is a first integral of the system

$$\dot{r} = u(r) = f(r)/r, \quad \dot{z} = w(r, z) = w_o(r) - zf'(r)/r, \quad (2.25)$$

and therefore level curves of $\chi(r, z)$ coincide with the streamlines.

Once the f function has been obtained, the linear equations (2.18) and (2.19) for the azimuthal and axial velocities v and w_0 can be easily solved and their contribution to the wall shear stresses determined. We show in §4.3 that w_0 can exhibit singular behaviour at selected values of F .

3. The low-Reynolds-number limit

Simplification of equation (2.17) for $f(r)$ is obtained by introducing the independent variable $x = (r/r_o)^2$ and the dependent variable $g(x) = f(r)/F$. The equation for $g(x)$ then reads

$$(xg'')' + \epsilon(g'^2 - gg'') = \tilde{\beta}; \quad g(x_i) = -1, \quad g(1) = g'(x_i) = g'(1) = 0, \quad (3.1)$$

where $\epsilon = F/2$ and $\tilde{\beta} = r_o^4\beta/8F$. The limit $F \rightarrow 0$ for which $\epsilon \rightarrow 0$ is regular and (3.1) is solvable order by order by developing both g and $\tilde{\beta}$ as regular expansions in powers of ϵ . The result up to second order in F is

$$\beta = AF[1 + BF + O(F^2)], \quad A = -16(1 - \eta)^3 \ln \eta^2 / ((1 + \eta)\lambda), \quad (3.2)$$

$$B = [3(1 + \eta^2)(1 + \eta^4) \ln^3 \eta^2 + 22(1 - \eta^2)(1 + \eta^2 + \eta^4) \ln^2 \eta^2 + 72(1 - \eta^2)^3 + 63(1 - \eta^2)^2(1 + \eta^2) \ln \eta^2] / (2(1 - \eta^2) \ln \eta^2 \lambda^2), \quad (3.3)$$

$$f(r) = F(p_{0,0}(x) + p_{0,1}(x) \ln x) + F^2(p_{1,0}(x) + p_{1,1}(x) \ln x + p_{1,2}(x) \ln^2 x) / 2 + O(F^3), \quad (3.4)$$

where $\lambda = 2(1 - \eta^2) + (1 + \eta^2) \ln \eta^2$. Explicit formulae for the polynomials $p_{i,j}(x)$ are given in Appendix A.

The above results corroborate the findings of Terrill (1967), and he observed that carrying out the analysis to higher-order would be extremely complicated. With the advent of symbolic manipulators these higher order corrections can be relegated to a computer. For $\eta = 0.5$ we have computed the series up to fourth order using Mathematica. The fourth-order expansions reproduce the numerically computed results for β only for $|F| \ll 1$, the series converge very slowly, and the series diverge for values of $|F|$ not much greater than 1. The slow convergence of the suction Reynolds number expansion is similar to the slow convergence of the extensional Reynolds number expansion encountered by Brady & Acrivos (1981).

The behaviour of the expansions (3.2) and (3.4) as a function of η may be understood by plotting the dependence of A and B on η as in figure 1. Both functions are bounded in $[0, 1]$, but for $\eta \rightarrow 0$ the slopes are infinite, exhibiting strong variations near $\eta = 0$. In §3.1 we show that the limit $\eta \rightarrow 0$ is singular and requires special attention. In the narrow gap limit, $\eta \rightarrow 1$, both functions $A(\eta)$ and $B(\eta)$ tend to zero, yielding the trivial solution $\beta = f = 0$. The correct result, obtained by a rescaling of the Reynolds number, is reported in §3.2.

For comparison with the results to be given in §3.1 for the singular case $\eta = 0$, the leading behaviours for $f(r)$ and the solution parameters for $\eta \rightarrow 0$ computed from the regular low Reynolds number expansions (3.2) and (3.4) are

$$f(r) = -(r^2 - 1)^2 F - r^2 [(1 - r^2)(7 - r^2)(2 + r^2) + 36 \ln r] F^2 / 36 + O(F^3), \quad (3.5)$$

$$\beta = -16F + 12F^2 + O(F^3), \quad \Sigma_i \rightarrow \infty, \quad \Sigma_o = -8F + 8F^2/3 + O(F^3). \quad (3.6)$$

3.1. The line source/sink limit

In the limit $\eta \rightarrow 0$, the flow is generated by a line source ($F > 0$) or sink ($F < 0$) on the cylindrical axis in which case $u(r) \rightarrow \infty$ as $r \rightarrow 0$ and hence $F = r_i U_i / \nu$ is

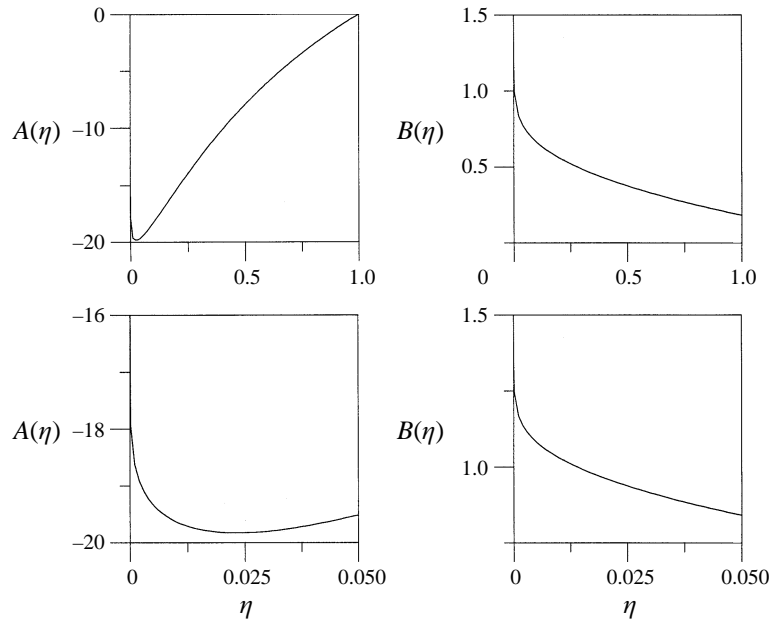


FIGURE 1. Coefficients A and B in the β development in equation (3.2) for the low-Reynolds-number limit. Both functions exhibit singular behaviour as $\eta \rightarrow 0$. The values at $\eta = 0$ are $A = -16$, $B = 3/2$.

undetermined. But F can still be defined as the radial volume flux per unit axial length (with a 2π factor in order to match the foregoing definition), namely

$$F = \frac{-1}{2\pi} \lim_{r \rightarrow 0} \int_0^1 2\pi r u(r) dz = -f(0). \quad (3.7)$$

The change of variable $x = (r/r_i)^2$ is no longer possible, so we take simply $x = r^2$ and $g(x) = f(r)/F$. Once again equation (3.1) is obtained, but now with $\epsilon = F/2$, $\tilde{\beta} = \beta/8F$, and with revised boundary conditions leading to the boundary-value problem

$$(xg'')' + \epsilon(g'^2 - gg'') = \tilde{\beta}; \quad g(0) = -1, \quad g(1) = g'(1) = 0, \quad g'(0) \text{ finite}. \quad (3.8)$$

The limit $\eta \rightarrow 0$ is singular since the highest derivative in g is multiplied by x , which is zero at the beginning of the interval. The solution can be obtained order by order, developing both g and $\tilde{\beta}$ in powers of ϵ as in Appendix A, but now the solution no longer involves logarithmic terms. In terms of the primary variables, we have

$$f(r) = -(1-r^2)^2 F + r^2(1-r^2)^2(4-r^2)F^2/36 - r^2(1-r^2)^2(9+23r^2-13r^4+r^6)F^3/5400 + \dots, \quad (3.9)$$

$$\beta = -16F + 4F^2 - 32F^3/135 + 194F^4/14175 + \dots, \quad (3.10)$$

$$\Sigma_i = 0, \quad \Sigma_o = -8F + 2F^2/3 - 4F^3/135 + \dots \quad (3.11)$$

To obtain Σ_i we have used the definition of the shear stress $\tau_{rz} = Dw = -zD(f'/r)$; w has an extremal value on the axis, due to the axisymmetry of the problem, and hence $\Sigma_i = 0$. While the leading terms of f , β , Σ_o are identical to those in (3.6), all higher-order terms are different. Mathematically, this is the result of a non-uniform double limit: in the previous section the limit $F \rightarrow 0$ was taken first, followed by the

limit $\eta \rightarrow 0$; here the order is reversed and a different result is obtained. Physically, this corresponds to the fact that the axial velocity must be zero on the surface of the inner cylinder, but is generally non-zero on the axis when that cylinder is replaced by a line source or sink. This change in w is reflected dramatically by the inner stress parameter Σ_i , which changes from 0 to ∞ .

3.2. The narrow-gap limit

The limit $\eta \rightarrow 1$ corresponds to the situation where both the inner and outer cylinder radii tend to infinity, and the effect of curvature on the fluid flow vanishes. The source Reynolds number F we have used previously is meaningless, because $F = -r_i U_i / \nu \rightarrow \infty$ for any non-zero value of the radial outflow velocity U_i . Accordingly, $R = -U_i d / \nu$ is introduced as the appropriate Reynolds number in the narrow gap limit. We introduce also the radial coordinate $x \in [0, 1]$ through $r = r_i + x$ and the new dependent variable $g(x) = f(r_i + x) / (r_i R)$ so that the meridional velocities remain finite as $r_i \rightarrow \infty$:

$$u(r) = \frac{R g(x)}{1 + x/r_i} \rightarrow R g(x), \quad w(r, z) = -\frac{R z g'(x)}{1 + x/r_i} \rightarrow -R z g'(x). \tag{3.12}$$

The boundary-value problem for $g(x)$ is then

$$g''' + R(1 + \epsilon x)(g'^2 - g g'') + \epsilon(2x g''' - g'' + R g g') + \epsilon^2(x^2 g''' - x g'' + g') = \tilde{\beta}(1 + \epsilon x)^3, \\ g(0) = -1, \quad g'(0) = g(1) = g'(1) = 0, \tag{3.13}$$

where $\epsilon = 1/r_i$ and $\tilde{\beta} = \beta/R$.

The low Reynolds number case can be handled as in the introduction to §3 and §3.1. Now, however, we posit a development in two small parameters, R and ϵ , according to

$$g(x) = \sum_{m,n=0}^{\infty} \epsilon^m R^n g_{m,n}(x), \quad \tilde{\beta} = \sum_{m,n=0}^{\infty} \epsilon^m R^n \beta_{m,n}. \tag{3.14}$$

The solutions are easily obtained order by order, with leading behaviours given by

$$g(x) = -1 + 3x^2 - 2x^3 - x^2(1 - x)^2 \epsilon \\ + \frac{1}{70} x^2(1 - x)^2(19 - 5x + 6x^2 - 4x^3)R + O[(\epsilon + R)^2], \tag{3.15}$$

$$\beta = -12R + 6\epsilon R + \frac{81}{35}R^2 - \frac{14}{5}\epsilon^2 R - \frac{81}{5}\epsilon R^2 - \frac{2929}{53900}R^3 \\ + \frac{6}{5}\epsilon^3 R + \frac{177}{100}\epsilon^2 R^2 + \frac{6477}{107800}\epsilon R^3 - \frac{398371}{147147000}R^4 + O[(\epsilon + R)^5]. \tag{3.16}$$

These solutions for $g(x)$ and β are compared with the low-Reynolds-number numerical results in figure 2 for the narrow gap radius ratio $\eta = 0.95$ ($\epsilon = 1/19$).

Results for source flow through one of two flat parallel plates can be immediately obtained upon setting $\epsilon = 0$ in the previous expressions, since in this limit curvature effects are removed. For example, the pressure gradient parameter is

$$\beta = -12R + \frac{81}{35}R^2 - \frac{2929}{53900}R^3 - \frac{398371}{147147000}R^4 + O(R^5). \tag{3.17}$$

Similar results have been reported by Terrill (1967) but here we have carried out the solution to much higher order in both R and ϵ .

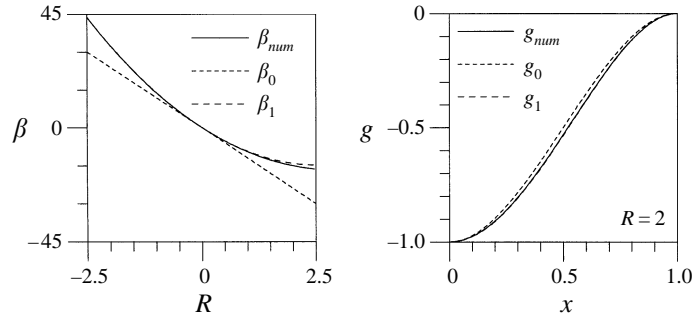


FIGURE 2. Comparison of the asymptotic and numerical values of β and $g(x)$ in the narrow gap limit at $\eta = 0.95$ for which $\epsilon = 1/19$; subscripts 0 and 1 refer to terms linear and quadratic in R in equations (3.15) and (3.16).

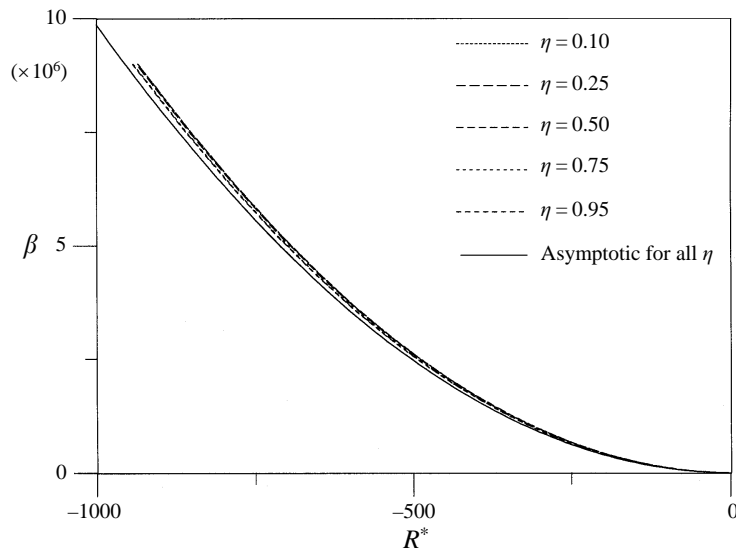


FIGURE 3. Pressure gradient parameter β as a function of the reduced Reynolds number $R^* = (1 - \eta)F/(1 + \eta)$ for different gaps. The asymptotic curve is $\pi^2 R^{*2}$.

4. Source flow at the inner wall

4.1. Numerical solutions

Results are now presented for radius ratio $\eta = 0.5$ to exhibit basic features of the flow. The high-Reynolds-number asymptotic analysis to be given in §4.2 suggests that the modified porous Reynolds number $R^* = F(1 - \eta)/(1 + \eta)$ may furnish a scaling law for β nearly independent of the radius ratio η , namely $\beta = \pi^2 R^{*2}$. Figure 3 shows β for different values of η , plotted against R^* . Indeed, the curves are remarkably tightly bound for all values of R^* .

Figures 4 and 5 show the dependence of the shear stress parameters Σ_i and Σ_o on R^* . Note that both parameters have been scaled with suitable functions of η suggested by the asymptotic analysis. The numerical results show that, for $|R^*| \gg 1$, Σ_i grows linearly with R^* and Σ_o follows an $|R^*|^{3/2}$ law, in agreement with the asymptotic analysis. In contrast to β , the scaled shear stress parameters become strongly η -dependent as $R^* \rightarrow 0$ as may be seen from the detailed inset in figure 4.

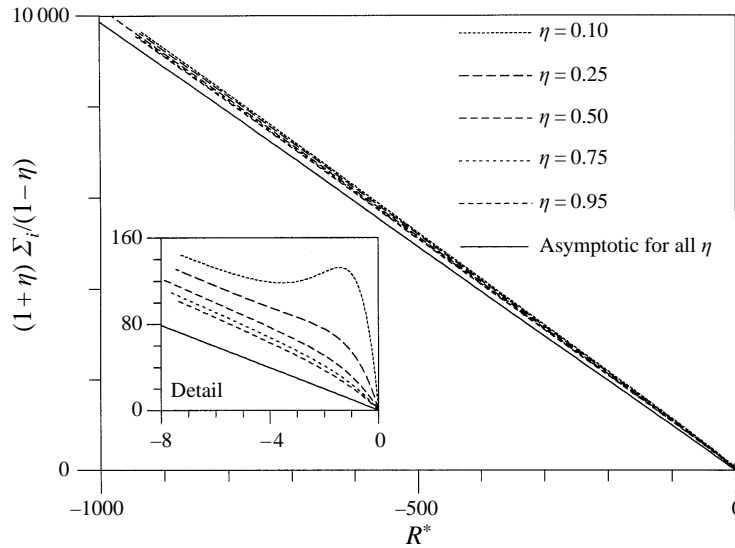


FIGURE 4. Scaled inner shear stress parameter $(1 + \eta)\Sigma_i/(1 - \eta)$ as a function of R^* for different gaps. The asymptotic curve is $-\pi^2 R^*$.

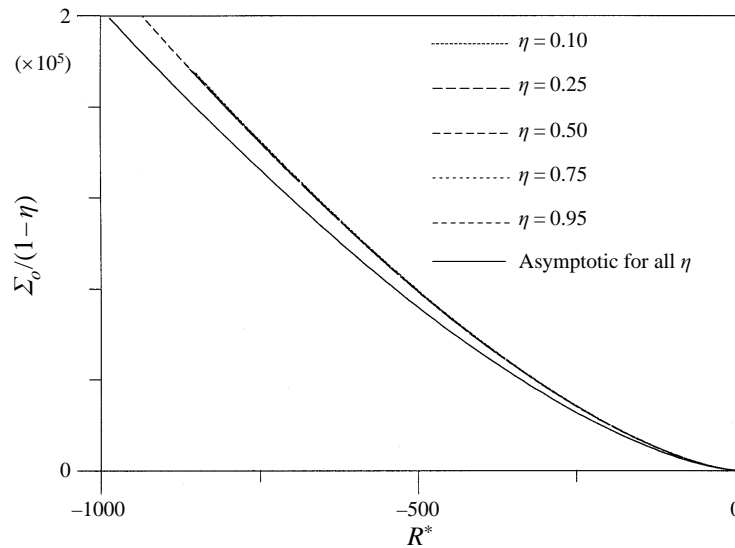


FIGURE 5. Scaled outer shear stress parameter $\Sigma_o/(1 - \eta)$ as a function of R^* for different gaps. The asymptotic curve is $2(\pi|R^*|)^{3/2}/\sqrt{3}$.

The functions f , $u(r) = f/r$, $w_1(r) = -f'/r$, and f'' scaled with F are plotted in figure 6(c) for $\eta = 0.5$. The axial velocity $w_1(r)$ displayed in figure 6(c) clearly shows the development of a boundary layer at the outer cylinder, inside which the axial velocity is reduced from its maximum value to zero; higher derivatives of f show stronger variations inside the boundary layer (figure 6d).

4.2. The high-Reynolds-number limit

In order to simplify equation (2.17) and display solution dependence on F , we introduce new independent $x = (r/r_i)^2$ and dependent $g = f/|F|$ variables. The

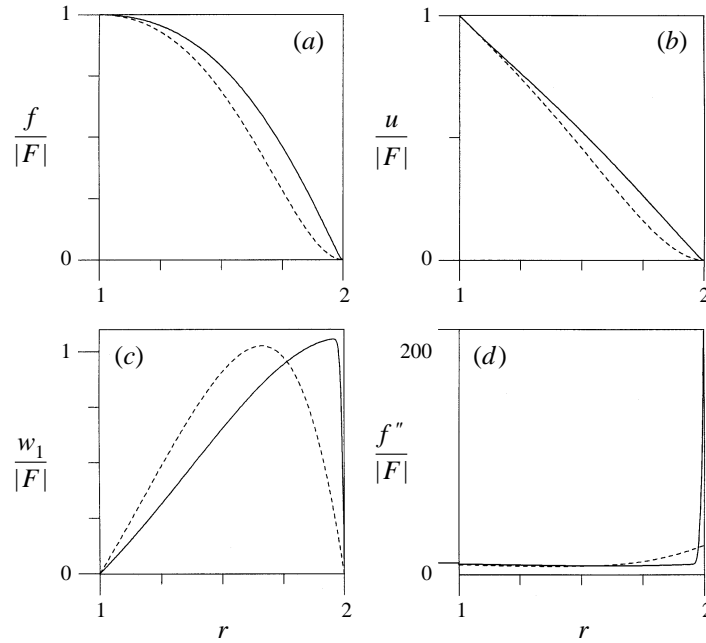


FIGURE 6. Distributions of f , u , w_1 , and f'' at $\eta = 0.5$ for $F = -20$ (dotted line) and $F = -5000$ (continuous line) showing the formation of a boundary layer on the outer cylinder.

boundary-value problem for $g(x)$ is then

$$\epsilon(xg'')' + g'^2 - gg'' = \tilde{\beta}, \quad g(1) = 1, \quad g(x_o) = g'(1) = g'(x_o) = 0, \quad (4.1)$$

where $\epsilon = 2/|F|$, $\tilde{\beta} = r_i^4 \beta / (4F^2)$, $x \in [1, x_o]$ and $x_o = 1/\eta^2$. In the limit of infinite radial source flow, $F \rightarrow -\infty$ for which $\epsilon \rightarrow 0^+$, one is faced with a singular perturbation problem. The solution of (4.1) for $\epsilon = 0$, $g'^2 - gg'' = \tilde{\beta}$, satisfying $g'(\bar{x}) = 0$ for some \bar{x} is $g(x) = g(\bar{x}) \cos(p(x - \bar{x}))$, where $p = \tilde{\beta}^{1/2}/g(\bar{x})$. Then the regular solution of (4.1) can satisfy only the boundary conditions at $x = 1$, and a boundary layer must appear on the outer cylinder, in agreement with the numerical solution displayed in figure 6. Then the leading behaviour in ϵ of the regular solution is

$$g_{\text{reg}}(x) = \cos(\tilde{\beta}^{1/2}(x - 1)). \quad (4.2)$$

These trigonometric (sine or cosine) functions of the wall-normal coordinate squared are the generic leading-order behaviours for flow in the inviscid region with blowing through porous walls; they have appeared in earlier studies for flow inside a cylinder (Yuan & Finkelstein 1956), between parallel plates (Proudman 1960), inside an annulus (Terrill 1967), and for radial stagnation flow impinging on a cylinder (Cunning *et al.* 1998). The agreement between solution (4.2) and the numerically computed one is extremely good, as can be seen in figure 7, with differences only very near the outer wall, in the boundary layer region. Since this layer shrinks to zero asymptotically as $\epsilon \rightarrow 0$, the dominant term for β

$$\tilde{\beta}^{1/2}(x_o - 1) \simeq \pi/2 \quad \Rightarrow \quad \beta \simeq \left(\frac{\pi(1 - \eta)}{1 + \eta} \right)^2 F^2 = \pi^2 R^{*2}, \quad (4.3)$$

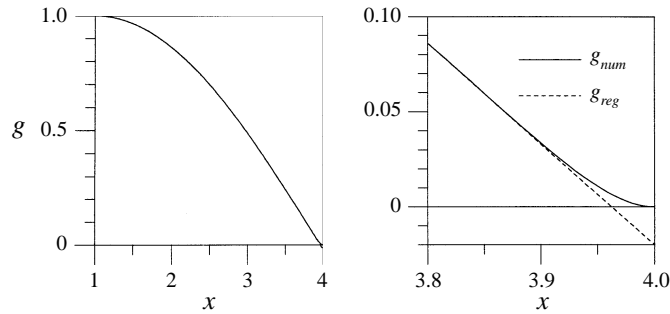


FIGURE 7. Comparison between the regular asymptotic solution and the numerically computed one for $\eta = 0.5$ at $F = -4460$. They differ only inside the boundary layer.

is in good agreement with the numerical results. The coefficient of R^{*2} in a parabolic fit of the numerically computed curves for $R^* \in [0, 6.E4]$ at $\eta = 0.5$ is 9.889, while the asymptotic value is $\pi^2 = 9.870$, with a relative error less than 0.2%.

In order to solve for the boundary layer structure on the outer cylinder, boundary layer variables X and G

$$x = (1 - \delta_1 X)/\eta^2, \quad g_{bl}(x) = \delta_2 G(X), \tag{4.4}$$

are introduced with small scaling parameters $\delta_1(\epsilon)$ and $\delta_2(\epsilon)$ to be determined. Now the equation for G is

$$A[-G''' + \delta_1(XG'')] + B[G'^2 - GG''] = 1; \quad G(0) = G'(0) = 0, \tag{4.5}$$

where $A = \epsilon\eta^4\delta_2/(\tilde{\beta}\delta_1^3)$ and $B = \eta^4\delta_2^2/(\tilde{\beta}\delta_1^2)$. The distinguished limit is obtained by taking $A = B = 1$; other possibilities give results that do not match with the numerically computed ones. This yields

$$\delta_1 = \eta\tilde{\beta}^{-1/4}\epsilon^{1/2}, \quad \delta_2 = \tilde{\beta}^{1/4}\epsilon^{1/2}/\eta, \tag{4.6}$$

and the differential equation for G inside the boundary layer at leading order in ϵ is

$$G''' - G'^2 + GG'' = -1; \quad G(0) = G'(0) = 0. \tag{4.7}$$

Equation (4.7) is similar to other boundary layer equations found in stagnation-point flows, such as those discussed in Chapter IX of Schlichting (1968). Although an explicit solution is not available, a detailed inspection of the numerical solutions obtained in §4.1 reveals that the term GG'' is considerably smaller than the other terms in the equation, and tends to zero uniformly at both the inner and outer edges of the boundary layer. Therefore, solutions of

$$G''' - G'^2 = -1; \quad G(0) = G'(0) = 0 \tag{4.8}$$

could provide an approximate description of the boundary layer structure that retains the essential qualitative features of the problem, as will be demonstrated later. It is now possible to solve for the approximate boundary layer structure described by equation (4.8) and match it to the regular solution in order to fix all the integration constants and $\tilde{\beta}$. Details of the solution to this equation are relegated to Appendix B where it is shown that at leading order in ϵ

$$G(X) = \begin{cases} X + 2\sqrt{3} - 3\sqrt{2} \tanh[\ln(\sqrt{2} + \sqrt{3}) + X/\sqrt{2}], & X = O(1) \\ X + 2\sqrt{3}, & X \gg 1, \end{cases} \tag{4.9}$$

$$G'(X) = 1 - 3/\cosh^2[\ln(\sqrt{2} + \sqrt{3}) + X/\sqrt{2}], \quad \forall X, \tag{4.10}$$

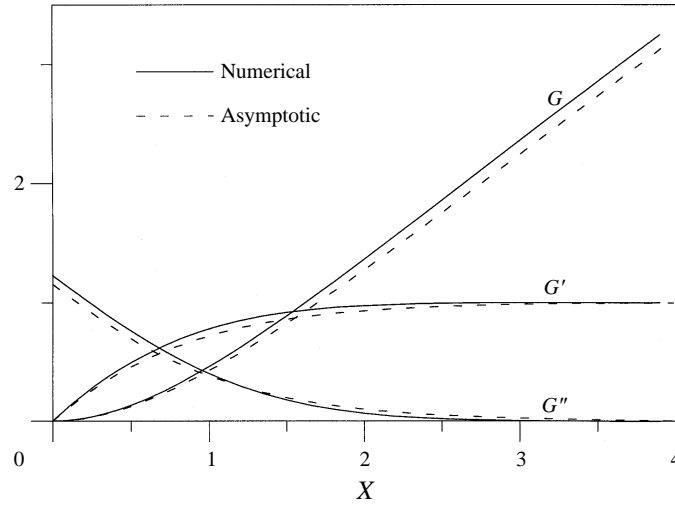


FIGURE 8. Comparison of the asymptotic boundary layer solution (B 3), (B 4), and (B 5) with the numerically computed results at $\eta = 0.5$ and $F = -4460$.

where the relationship between X and the radial coordinate r is

$$r^2 = r_o^2 [1 - (2\epsilon(1 - \eta^2)/\pi)^{1/2} X], \quad (4.11)$$

and the size of the boundary layer in the X variable is $(1/\sqrt{2})\ln(1/\epsilon)$ (equation (B 15)). Transforming back to the dimensionless radial coordinate r , one finds that the boundary layer thickness scales with R^* according to

$$\delta_{BL} \simeq \left(\frac{(1 + \eta)\epsilon}{4\pi(1 - \eta)} \right)^{1/2} \ln \frac{1}{\epsilon} \simeq \frac{\ln |R^*|}{(2\pi |R^*|)^{1/2}}. \quad (4.12)$$

Figure 8 shows a comparison between the boundary layer solution numerically computed and the approximate explicit solution obtained above at $\eta = 0.5$ and $F = -4460$. The agreement is quite satisfactory.

The inner and outer wall shear stress parameters can now be easily obtained. Σ_i is computed from the regular solution and Σ_o is found from the dominant solution in the boundary layer. The asymptotic results

$$\Sigma_i = \frac{1 - \eta}{1 + \eta} \pi^2 |R^*|, \quad \Sigma_o = \frac{2\pi^{3/2}}{\sqrt{3}} (1 - \eta) |R^*|^{3/2} \quad (4.13)$$

are in quite good agreement with the numerical computations, as can be seen in figures 4 and 5, considering that the term GG'' in equation (4.7) has been suppressed. The deviation between the approximate asymptotics and the high-Reynolds-number numerical calculations for Σ_i and Σ_o is 4% and 17%, respectively. These shear stress parameters provide a more sensitive test of the approximate asymptotics because they are calculated from local derivatives, whereas β is a global parameter.

4.3. The effects of translation, rotation, and external pressure gradient

The effects of the rotation of the inner and outer cylinder, the axial translation of the inner cylinder, and an external axial pressure gradient on blowing through the inner cylinder can now be examined. Since equations (2.18) and (2.19) are linear, we solve the four cases separately, remembering that the general solution is then obtained by

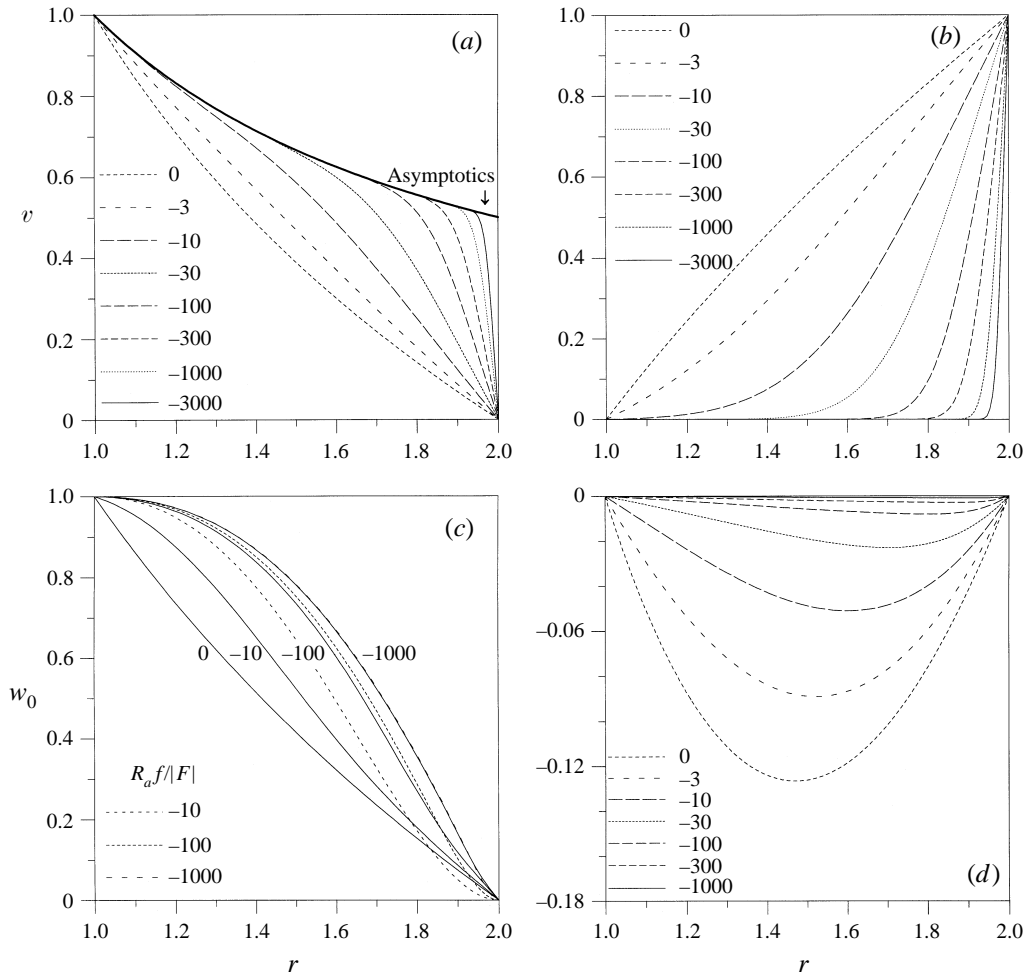


FIGURE 9. Effect of cylinder rotation, cylinder translation, and axial pressure gradient in the blowing case for different values of F . Distributions of (a) azimuthal velocity $v(r)$ for $R_i = 1$, (b) $v(r)$ for $R_o = 1$, (c) axial velocity $w_0(r)$ and distributions of $R_a f(r)/|F|$ for $R_a = 1$, and (d) $w_0(r)$ for $P = 1$.

superposition. Results for each of the R_i , R_o , R_a and P set equal to 1 separately, with the remaining parameters equal to zero, are displayed in figure 9 for different values of F at the selected value $\eta = 0.5$.

The effects of inner and outer cylinder rotation, presented respectively in figures 9(a) and 9(b), show the development of a boundary layer in the azimuthal velocity at large values of F . Outside this boundary layer v is independent of F . This is easily understood by inspection of equation (2.18), using the result from §4.2 that f is proportional to F at large F , which shows that the dominant term of the regular solution satisfies

$$D_+ v = 0, \quad v(r_i) = R_i \quad \Rightarrow \quad v(r) = R_i \frac{r_i}{r}. \tag{4.14}$$

This $1/r$ irrotational vortex solution guarantees that the angular momentum $rv(r)$ is conserved and only changes when the fluid particles get blown very near the outer cylinder where viscous effects come into play. In the special case $R_i = 0$ in figure 9(b), the inner cylinder is at rest, and the azimuthal velocity at large F is everywhere zero

except near the outer cylinder. A similar structure of the azimuthal velocity field has been reported by Cuning *et al.* (1998) for external radial stagnation flow impinging on a rotating cylinder in the limit of large blowing.

The effect of axial sliding is shown in figure 9(c). At large blowing, the solution for w_0 mimics f itself (cf. figure 6a). This may be understood by considering equation (2.19) governing w_0 in the limit $F \rightarrow \infty$ which has the leading-order behaviour

$$f'w_0 - fw_0' = 0 \quad \Rightarrow \quad w_0 \propto f \quad \Rightarrow \quad w_0(r) = R_a f(r)/|F| \quad (4.15)$$

obtained using boundary conditions on both f and w_0 . Figure 9(c) also exhibits the function $f(r)/|F|$ (dashed lines) for $F = -10, -100$, and -1000 , and for this last value the curves for w_0 and $f/|F|$ are almost coincident.

Finally, the effect of an external axial pressure gradient is shown in figure 9(d). The solution for $w_0(r)$ tends to zero as $F \rightarrow -\infty$, in accordance with equation (4.15). The classical parabolic Poiseuille profile at $F = 0$ is altered at finite values of F . Moreover, at large $|F|$ the quadratic pressure proportional to β ultimately swamps the effect of any fixed external pressure gradient. One must bear in mind that w_0 is the axial velocity component arising from an external axial pressure gradient and/or a sliding inner cylinder, and that the total axial velocity is computed from $w(r, z) = w_0(r) - zf'/r$.

Another effect of the external axial pressure gradient is to shift the stagnation circle at the outer cylinder wall axially away from $z = 0$. The velocity components u, w and the derivative Du are zero at the outer cylinder. Defining the stagnation point as the only point at the outer wall where a streamline has finite inclination to the wall, we arrive at $Dw = 0$, which gives $z_{sp} = r_o w_0'(r_o)/f''(r_o)$, where the subscript sp denotes stagnation point. The attachment angle α_{sp} (or detachment angle in the case of source flow at the inner wall) of the stagnation streamline at $r = r_o$ is now easily computed:

$$\tan \alpha_{sp} \equiv \lim_{r \rightarrow r_o} \frac{w(r, z_{sp})}{u(r)} = \frac{D^2 w}{D^2 u} \Big|_{r=r_o} = \frac{(rw_0'' + 2w_0')f'' - rw_0'f'''}{(f'')^2} \Big|_{r=r_o}. \quad (4.16)$$

Evaluation of (4.16) in the low- F limit, obtained with the aid of results given in §3 and Appendix A, furnishes

$$z_{sp} = [c_1(\eta)P + c_2(\eta)R_a]/F, \quad \tan \alpha_{sp} = c_3(\eta)R_a/F. \quad (4.17)$$

The expressions for $c_i(\eta)$ are given at the end of Appendix A. The leading-order high-Reynolds-number behaviour, found using the leading term for w_0 in (4.15), is given by

$$z_{sp} = o(1/F), \quad \tan \alpha_{sp} = -r_o R_a/F. \quad (4.18)$$

For comparison, the inner wall boundary conditions show that all streamlines leave the inner cylinder uniformly at the angle $\alpha_i = -\tan^{-1} R_a/F$.

5. Sink flow at the inner wall

5.1. Numerical solutions

For suction at the inner wall with an impermeable outer wall and both cylinders stationary, we again have $R_i = R_o = R_a = P = F_o = 0$, but now $F_i = F > 0$. As with source flow at the inner wall, a stagnation circle appears at the outer wall, but now as a result of a local reverse radial stagnation flow; therefore, it should be anticipated that the axial motion towards the symmetry plane $z = 0$ moves against an adverse pressure gradient. Our numerical methods used to obtain solutions for the source

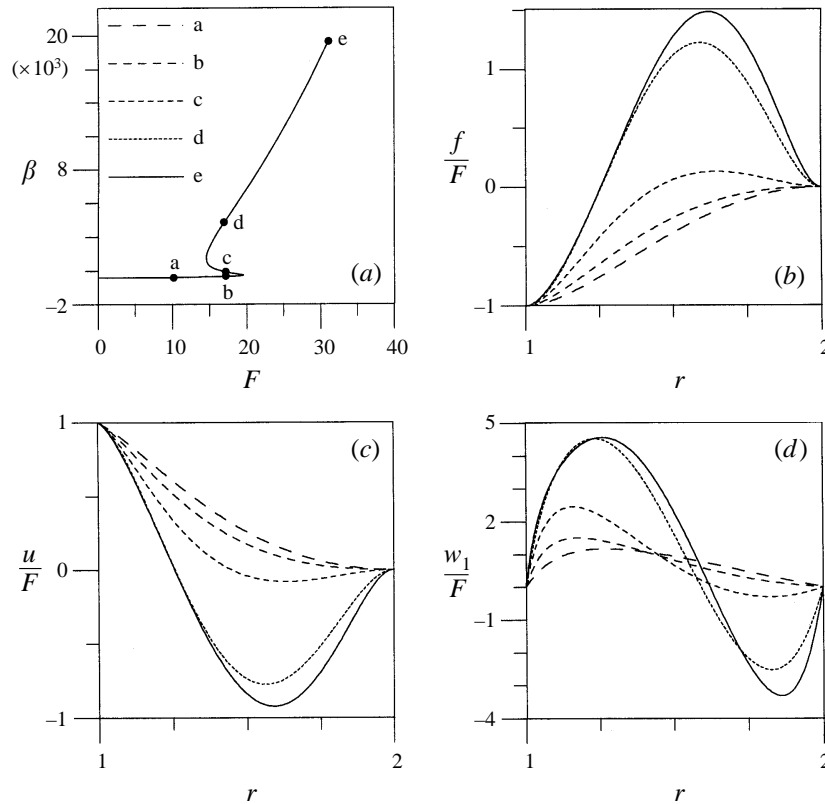


FIGURE 10. Variation of (a) the pressure gradient parameter β , (b) the similarity function f , (c) the radial velocity u , and (d) the axial velocity w_1 in the neighbourhood of the turning points for sink flow at $\eta = 0.5$.

flow can also be used in the present case. The nature of solutions over a wide range of suction Reynolds numbers at $\eta = 0.5$ will be presented first, followed by a study of the dependence on η .

The numerical results obtained for sink flow are qualitatively different from those obtained for source flow in §4. Figure 10(a) shows the pressure gradient parameter as a function of F . The first striking result is the appearance of two turning points at moderate values of F : three different solutions exist for all Reynolds numbers in the range $14.5 \leq F \leq 19.6$. Multiple solutions for f , u , and w_1 at $F = 17$ are plotted in figures 10(b), 10(c), 10(d), respectively, and corresponding streamline patterns are exhibited in figure 11. The flow experiences a drastic change as F evolves from the upper to the lower solution branch: a back-flow develops near the outer wall forming a recirculation cell above the dividing streamline. Thus the flow splits in two separate parts, and only fluid below the dividing streamline passes through the inner porous wall.

Another important difference between the source and sink flows is that in the former case only a single boundary layer appears adjacent to the outer cylinder, while in the latter case boundary layers appear on both cylinder walls. Therefore, it may be anticipated that the high-Reynolds-number asymptotics for the sink flow problem will be more complicated. These boundary layer structures can be seen in figure 12 which exhibits the axial velocity profile and the distribution of $f''(x)$ at $F = 200$

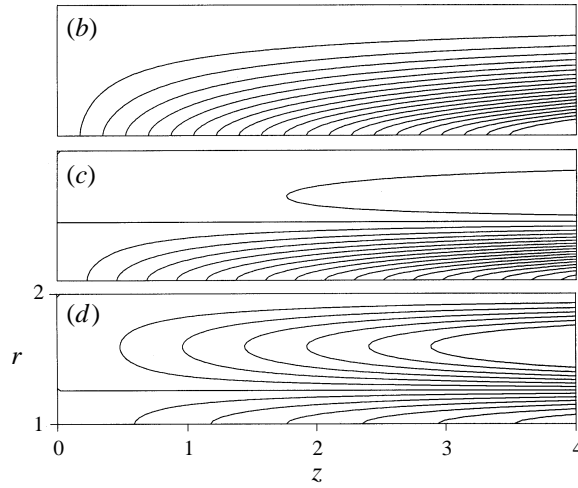


FIGURE 11. Streamline patterns for flow in the neighbourhood of the turning points for sink flow at $\eta = 0.5$, corresponding to figure 10, cases b, c and d.

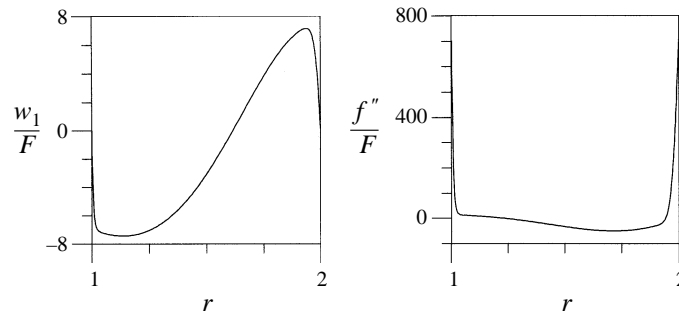


FIGURE 12. Axial boundary layer structure on the cylinder walls for sink flow at $\eta = 0.5$ and $F = 200$. The values of f'' at the walls are: $f''(r_i)/F = 1332$ and $f''(r_o)/F = 709$.

and $\eta = 0.5$. It is clear that the inner boundary layer is thinner than the outer one, and that $|f''|$ reaches its largest magnitude inside the inner boundary layer. Since the inner boundary layer is more intense than the outer one, the numerical computations at high Reynolds numbers are more difficult than for source flow through the inner cylinder.

5.2. The effect of radius ratio

The dependence of β on the modified suction Reynolds number R^* presented in figure 13(a, b) seems to exhibit similar behaviour at each value of η when R^* is large; β increases faster than in the source case, where the growth was quadratic in R^* .

For narrow gaps ($\eta \rightarrow 1$) the interval of triple solutions is reduced but never vanishes, as seen in figure 14(a). We have computed the solution of the equations at $\eta = 1$ (solid line) and the limit is smooth and regular. The suction Reynolds number F has been scaled as in §3.2.

For wide gaps ($\eta \rightarrow 0$), the behaviour of β is complex: the width of the region of triple solutions decreases until $\eta \approx 0.2$, then grows until $\eta \approx 0.01$, and finally shrinks to zero, as can be seen in figure 14(b). This is a reflection of the singular nature of

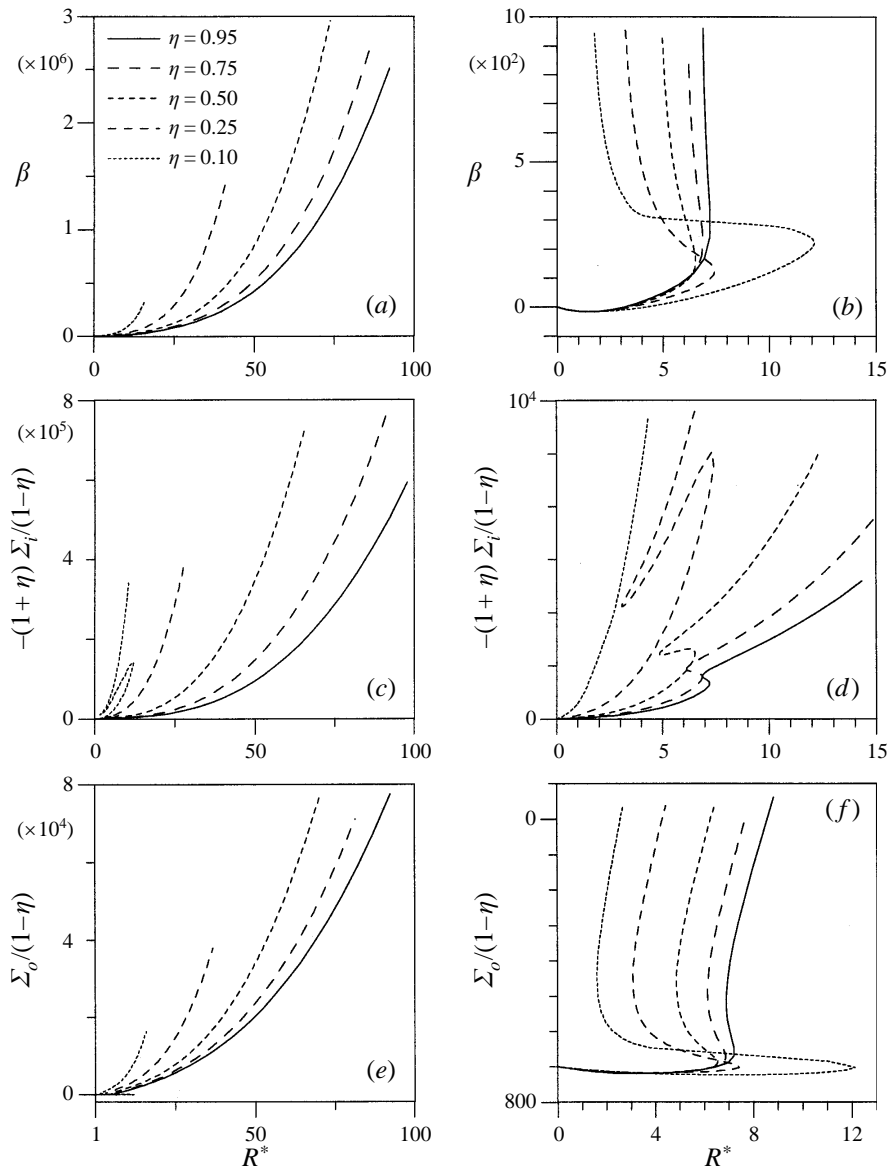


FIGURE 13. Parameter β , and scaled parameters Σ_i, Σ_o as functions of R^* for sink flow at different values of η . The plots in the second column show details in the neighbourhood of the turning points.

the $r_i \rightarrow 0$ limit already encountered in §3.1. The rapid change in solutions as $\eta \rightarrow 0$ is very similar to that already encountered in this limit when $F \rightarrow 0$ (cf. figure 1).

The scaled shear stress parameters as functions of the modified suction Reynolds number R^* are plotted in figure 13(c–f). At low values of R^* the curves exhibit the singular nature of the limit $\eta \rightarrow 0$ and at large values of R^* the shear stress curves at each η appear to have similar structure. For reasons discussed in the following section, we have not been able to determine an η scaling that reveals the apparent large R^* universal behaviour.

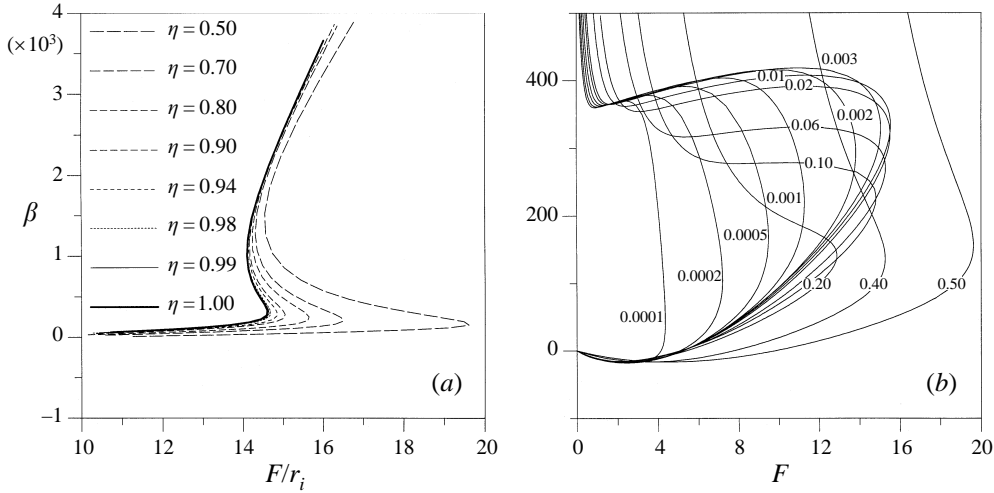


FIGURE 14. β as a function of F shown for the limiting cases: (a) $\eta \rightarrow 1$, (b) $\eta \rightarrow 0$.

5.3. The high-Reynolds-number limit

In the limit of large suction, $F \rightarrow +\infty$, the outer boundary layer and the intermediate regular solution can be obtained in the same way as for source flow. For the inner boundary layer we write $X = [(r/r_i)^2 - 1]/\epsilon$ and introduce $G(X) = f(r)/F$, where $\epsilon = 2r_i^2/F$, to obtain

$$G''' + \epsilon(XG'')' + G'^2 - GG'' = \tilde{\beta}, \tag{5.1}$$

$$G(0) = -1, \quad G'(0) = G(X_e) = G'(X_e) = 0, \tag{5.2}$$

in which $\tilde{\beta} = \epsilon^4\beta/16$, $X \in [0, X_e]$, and $X_e = (\eta^{-2} - 1)/\epsilon$. In the high-Reynolds-number limit $\epsilon \rightarrow 0^+$ the boundary-value problem describing the structure of the inner boundary layer becomes

$$G''' + G'^2 - GG'' = \tilde{\beta}, \quad G(0) = -1, \quad G'(0) = 0. \tag{5.3}$$

Numerical evaluation of the different terms comprising the solution of (5.3) are plotted in figure 15. It appears that no term can be neglected and, since we are unable to solve (5.3) in closed form, no explicit expressions for the asymptotic behaviours of β and f are available. Close scrutiny of figure 15 reveals two distinct regions inside the inner boundary layer: very near the wall only G''' and GG'' are important, while in the adjacent region all four terms in (5.3) are of comparable magnitude.

5.4. The effects of translation, rotation, and external pressure gradient

As in the blowing case, owing to linearity, we examine separately R_i , R_o , R_a and P equal to 1, setting the remaining parameters equal to zero, at the fixed value $\eta = 0.5$. In figures 16(a) and 16(b) the azimuthal velocity v is plotted as a function of r for different values of F . For moderate values of F , below the region of multiple solutions, the azimuthal velocities v lie between those for circular Couette flow (corresponding to $F = 0$) and the zero velocity of the outer cylinder; hence in this region suction reduces the influence of the rotating inner cylinder. In the region of multiple solutions, v changes drastically to the asymptotic solution for large F found in the blowing case, $v(r) = R_i r_i/r$, and a boundary layer appears at the outer wall. Curves labelled 17(b-d) in figure 16 refer to multiple solutions for $F = 17$ shown in figure 10.

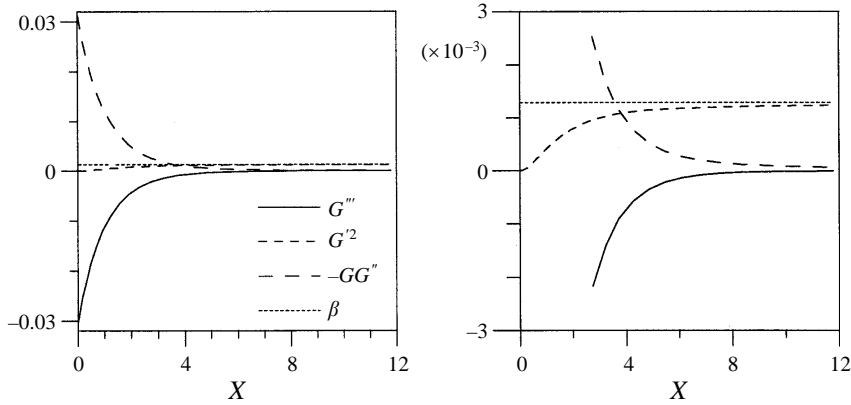


FIGURE 15. Distributions of the numerically computed terms appearing in the inner boundary layer equation (5.3) for sink flow at $\eta = 0.5$ and $F = 200$.

The effects of axial sliding and external axial pressure gradient are shown in figure 16(c, d). Again a drastic change takes place in the region of multiple solutions, but a new phenomena appears before reaching this region: w_0 blows up at $F = 9.865$. In order to understand this singular behaviour, we consider equation (2.19) rewritten here as

$$\mathcal{L}w_0 = D_+Dw_0 + \frac{1}{r}(f'w_0 - fw'_0) = P, \quad w_0(r_i) = R_a, \quad w_0(r_o) = 0. \quad (5.4)$$

This linear boundary value problem for w_0 depends nonlinearly on the parameter F , through the function f . For specific values of F , the homogeneous equation $\mathcal{L}w_0 = 0$, with boundary conditions $w_0(r_i) = w_0(r_o) = 0$, may have non-trivial solutions. These solutions are the eigenfunctions of \mathcal{L} , and the corresponding F -values are the eigenvalues, even though the F -dependence is nonlinear. The existence of an eigenvalue generally precludes a solution of equation (5.4) since solutions exist if and only if

$$P \int_{r_i}^{r_o} r\zeta(r)dr = r_i\zeta'(r_i)R_a, \quad (5.5)$$

where $\zeta(r)$ is the eigenfunction of the adjoint problem: $\mathcal{L}^*\zeta = 0$, $\zeta(r_i) = \zeta(r_o) = 0$. Therefore, when eigenvalues exist, equation (5.4) has no solution, except for combinations of R_a and P satisfying the Fredholm alternative (5.5). Over the large range of F examined in this paper, only the aforementioned eigenvalue $F = 9.865$ has been found at $\eta = 0.5$. One may wonder if a similar phenomenon occurs for $v(r)$. In this case it is possible to show that equation (2.18) is free of ‘nonlinear eigenvalues’ since the solution for $v(r)$ is explicitly given by

$$v(r) = \frac{C}{r} + \frac{D}{r} \int_{r_i}^r r' \exp\left(\int_{r_i}^{r'} \frac{1}{r''}f(r'')dr''\right)dr', \quad (5.6)$$

where the constants C and D are determined by the boundary conditions in (2.18). The integrand in (5.6) is positive, so the solution for C and D exists and is unique.

Thus w_0 , the part of the axial velocity independent of z , experiences two important changes when there is suction through the inner wall: the first occurs at the nonlinear eigenvalue $F = 9.865$ where w_0 becomes singular, and the second occurs at somewhat larger values of F where triple solutions appear. At large F , the suction drives w_0 to

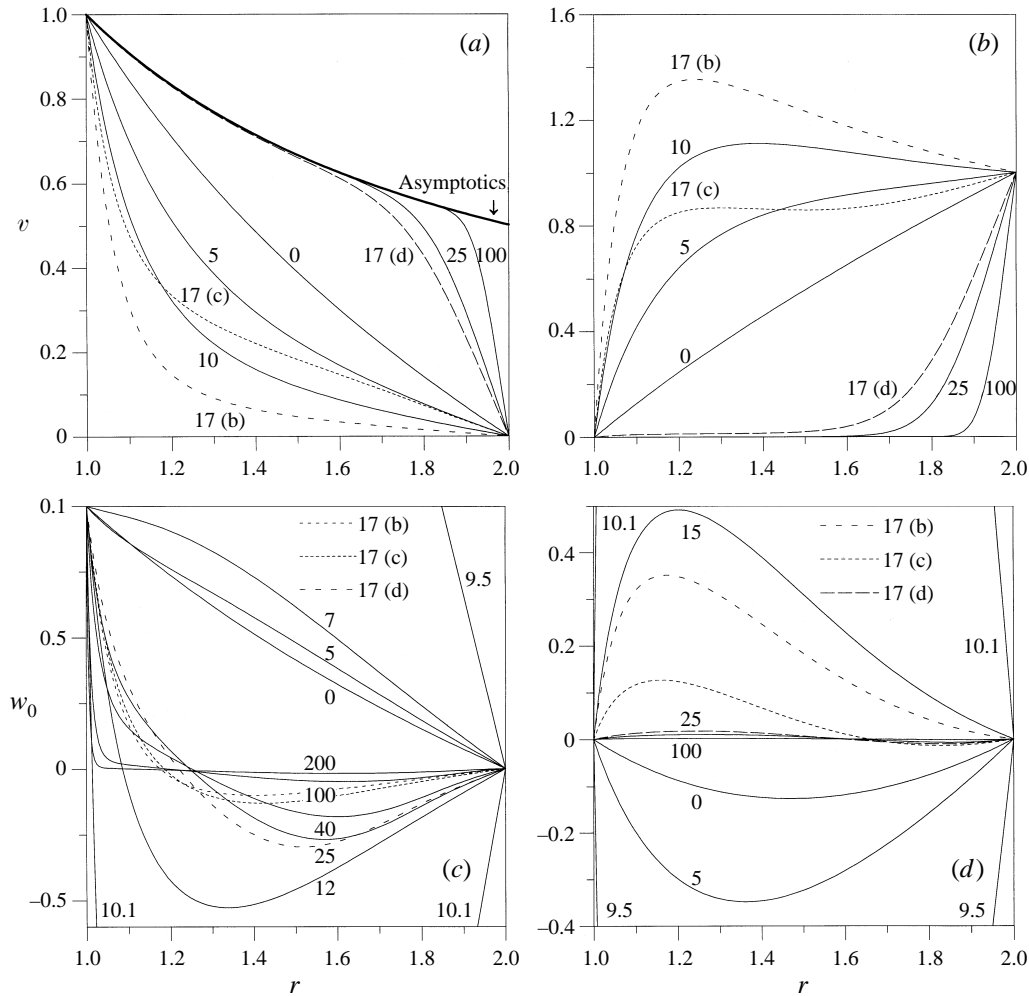


FIGURE 16. Effect of cylinder rotation, cylinder translation, and axial pressure gradient in the suction case. Distributions of (a) azimuthal velocity $v(r)$ for $R_i = 1$, (b) $v(r)$ for $R_o = 1$, (c) axial velocity $w_0(r)$ for $R_a = 1$, and (d) $w_0(r)$ for $P = 1$. Figures (c) and (d) exhibit the change in behaviour in $w_0(r)$ across the singular point $F = 9.865$.

zero, and the effect of axial sliding is confined to the boundary layer on the inner cylinder necessary to accommodate the boundary condition $w_0(r_i) = R_a$.

The position and angle of the stagnation point on the outer cylinder for inner wall suction are exactly those given by equations (4.17) and (4.18) originally found for inner wall blowing.

6. Summary and conclusion

The general similarity formulation for steady, swirling, Couette–Poiseuille flow in an annulus has been presented. The original study by Terrill (1967) was restricted to walls at rest, while here the most general boundary conditions compatible with the similarity formulation are included, namely rotation and axial translation of the cylinder walls, uniformly stretching and twisting cylinder walls, and an external

axial pressure gradient. The system of equations splits into two parts: the primary nonlinearly coupled equations governing the meridional flow driven by radial suction/blowing through the porous cylinder walls and the azimuthal flow driven by torsional stretching of the cylinder walls; the remaining equations linearly coupled to the primary equations govern the effects of cylinder translation and rotation and the effect of an external axial pressure gradient.

Fluid motion driven by uniform source or sink flow through a porous inner cylinder with an impermeable outer cylinder is analysed in detail. In this case the single primary equation depends on only two parameters, namely the radial flux Reynolds number F and the radius ratio η .

Regular low-Reynolds-number expansions confirm the results taken to second order by Terrill (1967). The higher-order terms computed here shows that the low-Reynolds number series is very slowly convergent. The singular limit $\eta \rightarrow 0$ has been analysed in detail. The narrow gap limit $\eta \rightarrow 1$ has also been studied, carrying the earlier results of Terrill (1967) to considerably higher order in the double expansion in powers of the gap size and Reynolds number. It is shown that this narrow-gap limit is regular.

Numerical solutions for blowing and suction through the inner wall have been obtained for $\eta = 0.1, 0.25, 0.50, 0.75$, and 0.95 starting from analytic Stokes flow solutions and proceeding to as high a Reynolds number as was computationally feasible with our collocation technique incorporating Chebyshev basis functions. Asymptotic expressions corroborating the numerical results are found in different limiting cases. These include high- and low-Reynolds-number limits, the narrow-gap limit, and the limit where the inner cylinder is replaced by a uniform line source.

For source flow through the inner wall solutions are unique up to the highest Reynolds number $F = -5000$ investigated. In this situation a forward radial stagnation flow is impressed on the outer cylinder where a stagnation circle appears at the symmetry plane. Fluid emitted radially through the inner cylinder fills the gap as it turns to flow uniaxially down the annulus. The axial (radial) velocity increases (decreases) monotonically to the edge of a boundary layer that forms on the outer cylinder at high Reynolds numbers, and then falls to zero to satisfy the impermeable no-slip boundary condition at the outer wall. No boundary layer forms on the inner cylinder wall through which the fluid is emitted. An approximate high-Reynolds-number analysis reveals simple scaling laws for solution parameters. In particular, the pressure gradient parameter exhibits the asymptotic behaviour $\beta = \pi^2 R^{*2}$, where $R^* = F(1 - \eta)/(1 + \eta)$. The analysis also shows that the inner wall shear stress grows linearly with R^* whilst the outer wall shear stress grows like $|R^*|^{3/2}$, as $R^* \rightarrow -\infty$. Analogous to results obtained for uniform blowing in channels and pipes, there are no regions where self-similar solutions do not exist.

The suction flow is found to be much more complex. Unique solutions at low Reynolds numbers evolve into a region of triple solutions at moderate Reynolds numbers, the size of which depends on η . At yet higher Reynolds number there emerges a unique solution with reverse flow. The back-flow splits the fluid motion into two cells that never mix across the dividing streamline $r = r_c$. In the inner cell, $r_i < r < r_c$, fluid arriving from upstream infinity turns smoothly to enter the inner cylinder through a boundary layer that develops on the inner wall. In the outer cell, $r_c < r < r_o$, the fluid recirculates, arriving from upstream infinity in the interior of the annulus and returning to upstream infinity along the outer cylinder wall where a second boundary layer is formed. The radial velocity is thus always negative in the inner cell and always positive in the outer cell. Of the two boundary layers, the one located at the inner cylinder is the most intense. Numerical computations suggest

that the high-Reynolds-number behaviour of the flow is similar at each η . The scaling that collapses results for the wall shear stresses and the pressure gradient parameter should be obtained through the high-Reynolds-number asymptotics, but the complex structure of the boundary layer at the inner cylinder makes the determination of the asymptotic behaviour difficult.

Multiple solutions appear to be a generic feature of these self-similar flows since they are also found at sufficiently large suction Reynolds number in porous tubes (Terrill & Thomas 1969) and in channels and tubes with accelerating walls (Brady & Acrivos 1981). A detailed analysis of the structure of flow generated by suction through the inner cylinder wall shows that the multiple solutions persist as $\eta \rightarrow 1$, but that they slowly vanish as $\eta \rightarrow 0$ in accord with the results of Banks & Zaturka (1992).

Solutions of the subsidiary equations are given for the selected value $\eta = 0.5$ to exhibit the influence of cylinder translation, cylinder rotation, and an axial pressure gradient on the source/sink flows. An unusual feature in the axial velocity generated by longitudinal motion of the inner cylinder is observed: at a single particular value of wall suction, w_0 becomes singular. This is connected with an isolated eigenvalue of the linear equation slaved to the primary flow solution. For blowing through the inner cylinder wall, on the other hand, the subsidiary equations give regular contributions to the total velocity field. Of the eleven parameters governing the flow, only R_a and P break the symmetry about the mid-plane at $z = 0$. For such flows the stagnation flow on the outer wall, forward for $F < 0$ and reverse for $F > 0$, is skewed to positive or negative values of z . In these cases we have derived explicit results for the displaced position z_{sp} of the stagnation circle at low values of $|F|$ and for the angle α_{sp} of flow attachment/detachment in both the low and high $|F|$ limits.

Of course one would like to ascertain the stability of the steady flows found in this investigation. Unfortunately, we cannot make any direct statement concerning our steady solutions based on the spatial stability results of Durlofsky & Brady (1984) because we do not have the requisite symmetry about the gap centreline. Nevertheless, the porous pipe results of Durlofsky & Brady (1984), and those of Banks & Zaturka (1992) for constant and equal mass flux through each cylinder wall, both show that for blowing there exists a unique stable branch, whereas for suction multiple solution branches appear which render the flow unstable. These findings are consistent with the general properties of dynamical systems (Guckenheimer & Holmes 1986): the development of two turning points corresponds to a saddle-node bifurcation where a real eigenvalue crosses the imaginary axis to produce a positive real part. It is therefore likely that the steady flows we have computed after the first turning point are unstable.

The stability of these similarity flows with respect to general three-dimensional perturbations is a much more difficult issue. The unbounded growth of the velocity field along the pipe and the convective transport of the perturbations make the analysis very hard. Similar difficulties appear in the analysis of combustion fronts, and many fundamental aspects of the instability theory in these problems remain unsolved (Kortsarts *et al.* 1997).

The solutions found for suction flow through the inner cylinder may have some bearing on the operation of rotating membrane separators. If indeed a recirculating cell persists in certain regions of parameter space with a net axial throughflow in a finite length apparatus, the efficiency of the dynamic filter device would certainly be compromised. Entrance effects, however, are likely to destroy the self-similar suction flow in the annulus at sufficiently large values of F , with or without an external axial

pressure gradient. Thus a spatial stability analysis of the suction similarity solutions will play a key role in determining optimum conditions for operation of rotating membrane separators.

This work was partially supported by DGICYT grant PB94-1209 and by DGICYES grant PR95-425 during F. Marquès' visit to the Department of Mathematics at The Pennsylvania State University in University Park, Pennsylvania, USA. The final version of the manuscript was put together while P. D. Weidman was on sabbatical leave at Laboratoire d'Hydrodynamique in Palaiseau, France, and the support of Ecole Polytechnique for this visit is very much appreciated.

Appendix A. Small- F expansions

In order to solve equation (3.1) at low transpiration Reynolds number we develop both g and $\tilde{\beta}$ as regular expansions in powers of ϵ as follows:

$$g(x) = \sum_{n=0}^{\infty} g_n(x)\epsilon^n, \quad \tilde{\beta} = \sum_{n=0}^{\infty} \beta_n\epsilon^n. \tag{A 1}$$

The boundary-value problem governing $g_n(x)$ is

$$(xg_n'')' = \beta_n + \sum_{m=0}^{n-1} (g_m g_{n-1-m}'' - g_m' g_{n-1-m}') = \beta_n + G_n(x), \tag{A 2}$$

$$g_n(e) = -\delta_{n,0}, \quad g_n(1) = g_n'(e) = g_n'(1) = 0, \tag{A 3}$$

where $e = x_o = \eta^2$. Integrating (A 2) we obtain

$$g_n(x) = a_n + c_n x + \beta_n x^2 / 2 + d_n x \ln(x) + h_n(x), \tag{A 4}$$

$$h_n(x) = \int^x \int^{x''} \frac{1}{x''} \int^{x'''} G_n(x') dx' dx'' dx'''. \tag{A 5}$$

The integrations in $h_n(x)$ are made without introducing integration constants, therefore $h_n(x)$ is free of terms 1, x , and $x \ln x$. The constants a_n , c_n , β_n , and d_n are easily obtained from the boundary conditions for g and the function h_n , which depends only on lower-order solutions g_k . Using induction on n , it is easy to show that

$$g_n(x) = \sum_{k=0}^{n+1} p_{n,k}(x) \ln^k(x), \tag{A 6}$$

where $p_{n,k}$ are polynomials in x of degree $2n - k + 2$, satisfying $p_{n,k}(0) = 0 \forall k \geq 1$. Therefore, computation of the expansions for $f(r)$ and β is purely an algebraic problem, although the expressions become highly cumbersome for $n \geq 2$, because the coefficients are involved functions of e . The expressions $p_{n,k}(x)$ for $n = 0, 1$ are

$$\begin{aligned} (1 - e)E p_{0,0} &= -2(1 - e) - y + 2(1 - e + y)x - yx^2, \quad E p_{0,1} = -2x, \\ 18(1 - e)^2 E^3 p_{1,0} &= -216(1 - e)^3 e + (1 - e)^2 e(1 - 71e)y + 4(1 - e)e(17 + 43e - e^2)y^2 \\ &\quad + 9e(1 + e)(2 + 3e)y^3 + [216(1 - e)^3(1 + e) + (1 - e)^2(215 - 136e + 71e^2)y \\ &\quad + (1 - e)(3 - 91e - 370e^2 + 4e^3)y^2 - 2(1 + e)(7 + 9e + 27e^2)y^3]x - 9[24(1 - e)^3 \\ &\quad + 5(1 - e)^2(5 - 3e)y + 2(1 - e)(1 - e - 11e^2)y^2 - (1 + e)(1 + 3e^2)y^3]x^2 \\ &\quad + y[10(1 - e)^2 + (1 - e)(17 + 5e)y + 6(1 + e)y^2]x^3 - y^2[2(1 - e) + (1 + e)y]x^4, \end{aligned}$$

$$\begin{aligned}
18(1-e)E^3 p_{1,1} &= -[216(1-e)^2(1+e) + (1-e)(143 + 350e + 71e^2)y \\
&\quad + 2(38 + 13e + 13e^2 + 2e^3)y^2 + 18(1+e)y^3]x + 72[6(1-e)^2 + (1-e)(5 + 3e)y \\
&\quad - (1+e)y^2]x^2 - 6y[2(1-e) + (1+e)y]x^3, \\
(1-e)E^2 p_{1,2} &= 2(1-e)x(1-x) + yx,
\end{aligned}$$

where $e = \eta^2$, $y = \ln e$, $E = 2(1-e) + (1+e)y$. The values of β_n for $n = 0, 1$ are

$$\beta_0 = -2y/[(1-e)E], \quad (\text{A } 7)$$

$$\begin{aligned}
\beta_1 &= [72(1-e)^3 + 63(1-e)^2(1+e)y + 22(1-e)(1+e+e^2)y^2 \\
&\quad + 3(1+e)(1+e^2)y^3]/[(1-e)^2E^3]. \quad (\text{A } 8)
\end{aligned}$$

For $\eta = 0.5$ we have carried out the algebraic computations up to fourth order ($n = 3$), and the scaled pressure gradient parameter to this order is

$$\tilde{\beta} = 0.496095 + 0.129460\epsilon + 0.307177 \times 10^{-2}\epsilon^2. \quad (\text{A } 9)$$

The limiting case $\eta \rightarrow 0$ is readily obtained because $e^p y^q \rightarrow 0$ if $p \geq 1$, and $x \rightarrow r^2$; in this limit the leading polynomials are simply

$$p_{0,0} = -(1-x)^2, \quad p_{0,1} = 0, \quad (\text{A } 10)$$

$$p_{1,0} = -x(1-x)(2+x)(7-x)/18, \quad p_{1,1} = -x, \quad p_{1,2} = 0. \quad (\text{A } 11)$$

To determine the position and angle of the stagnation streamline at the outer cylinder, values of w'_0 , w''_0 , f'' and f''' at r_o must be computed. From equation (2.19) the leading-order behaviour of w_0 for $|F| \ll 1$ is the basic Couette–Poiseuille solution (2.20) from which the derivatives

$$w'_0 = \left(\frac{1}{2(1-\eta)} + \frac{1+\eta}{4 \log \eta} \right) P + \frac{1-\eta}{\log \eta} R_a, \quad w''_0 = \left(\frac{1}{2} - \frac{1-\eta^2}{4 \log \eta} \right) P - \frac{(1-\eta)^2}{\log \eta} R_a \quad (\text{A } 12)$$

are obtained. The derivatives for f found using the leading term for g_0 in (A 6) are

$$f''(r_o) = 4Fg''_0(1)/r_o^2, \quad f'''(r_o) = (12Fg''_0(1) + 8Fg'''_0(1))/r_o^3, \quad (\text{A } 13)$$

and inserting both (A 12) and (A 13) into (4.16) gives the coefficients $c_i(\eta)$ in (4.17), namely

$$c_1(\eta) = \frac{-(1+\eta)E}{8(1-\eta)^3 y}, \quad c_2(\eta) = \frac{-(1+\eta)E}{2(1-\eta)(1-e+y)y}, \quad c_3(\eta) = \frac{(1+\eta)E}{(1-e+y)^2}, \quad (\text{A } 14)$$

with e , y , and E as previously defined in this Appendix.

Appendix B. Large-blowing asymptotics

To formally obtain the asymptotic behaviour as $F \rightarrow \infty$, the outer solution governed by (4.8) must be found and matched to the inner solution (4.2). A first integral of (4.8) is given by

$$\frac{3}{2}G'^2 = G'^3 - 3G' + \lambda = p(G'), \quad (\text{B } 1)$$

where λ is an integration constant, and the solution is reduced to quadratures involving elliptic functions. The final result depends on the roots of the third-order polynomial $p(G')$, which has one or three real roots depending on whether $\lambda > 2$ or $\lambda < 2$, respectively. At this point information gleaned from the numerical computations becomes essential. We find $\lambda = 3G''^2(0)/2 \simeq 2$, and for X very near zero, G , G' and G'' are positive. But in order to match the boundary layer solution with the outer

solution, we need $G'' < 0$. Therefore G'' must change sign, which means that $\lambda \lesssim 2$ and $p(G')$ has three real roots $r_1 < r_2 < r_3$ satisfying $r_1 \lesssim -2$, $r_2 \lesssim 1$, $r_3 \gtrsim 1$. Writing now $G' = r_1 + (r_2 - r_1) \sin^2 \phi$ we obtain the approximate boundary layer solution

$$X = [6/(r_3 - r_1)]^{1/2}(u - u_0), \tag{B 2}$$

$$G(X) = (r_3 - (r_3 - r_1)E/K)X - [6(r_3 - r_1)]^{1/2}(Z(u) - Z(u_0)), \tag{B 3}$$

$$G'(X) = r_1 + (r_2 - r_1)\text{sn}^2 u, \tag{B 4}$$

$$G''(X) = 2(r_2 - r_1)[(r_3 - r_1)/6]^{1/2}\text{sn } u \text{cn } u \text{dn } u, \tag{B 5}$$

where K and E are the complete elliptic integrals of the first and second kind, $Z(u)$ is Jacobi's Zeta function, $k^2 = (r_2 - r_1)/(r_3 - r_1) \lesssim 1$ is the elliptic parameter, and u_0 is obtained from the boundary conditions on G , namely, $\text{sn } u_0 = [-r_1/(r_2 - r_1)]^{1/2}$. Definitions and properties of the Jacobian elliptic functions $\text{sn } u$, $\text{cn } u$ and $\text{dn } u$ have been taken from Abramowitz & Stegun (1965).

By the method of matched asymptotic expansions (Bender & Orszag 1978), one must join the asymptotic behaviour of $G(X)$ for $X \gg 1$ with the regular Taylor series for $g_{\text{reg}}(x)$ about $x \simeq x_0$. But in our case G' , G'' , and the elliptic part of G are periodic, and the period tends to infinity as $k^2 \rightarrow 1$. On the other hand, inspection of the numerical solution shows that matching must occur in a narrow region where G'' changes sign. Therefore we will match the function and its derivatives up to second order at a point to be determined.

Let $\tilde{\beta}^{1/2}(x - 1) = \pi/2 - \delta_0$, $u = K + u_1$, and $r_2 = 1 - \delta$ be the values at the matching point, with δ_0 , u_1 , and δ to be determined. Using properties of the elliptic functions, the three matching conditions may be written

$$[6(r_3 - r_1)]^{1/2} \left\{ (r_3/(r_3 - r_1) - E/K)(K + u_1 - u_0) + Z(u_0) - Z(u_1) + k^2 \text{sn } u_1 \text{cn } u_1 / \text{dn } u_1 \right\} = (\sin \delta_0) / \delta_2, \tag{B 6}$$

$$r_1 + (r_2 - r_1) \text{cn}^2 u_1 / \text{dn}^2 u_1 = \cos \delta_0, \tag{B 7}$$

$$2(r_2 - r_1)(1 - k^2)[(r_3 - r_1)/6]^{1/2} \text{sn } u_1 \text{cn } u_1 / \text{dn}^3 u_1 = \delta_2 \sin \delta_0. \tag{B 8}$$

Assuming now $\delta \ll 1$, the leading behaviours of K , E , and the remaining two roots r_1 and r_2 are given by

$$r_1 = -2 + 1/3\delta^2 + O(\delta^3), \quad r_3 = 1 + \delta - 1/3\delta^2 + O(\delta^3) \tag{B 9}$$

$$K = \frac{1}{2} \ln \left(\frac{16}{1 - k^2} \right) + o(1), \quad E = 1 + o(1). \tag{B 10}$$

Assuming also that δ_0 and u_1 are vanishingly small, equations (B 6)–(B 8) require that

$$\ln(24/\delta) = \sqrt{2}\delta_0/\delta_2, \quad \delta_0^2 = 2\delta, \quad 2\sqrt{2}\delta u_1 = \delta_2\delta_0, \tag{B 11}$$

where some care is needed with the equation (B 7) because cancellations occur at leading order. These equations yield the values of δ , δ_0 , and u_1 as a function of ϵ because δ_2 is known at leading order in equation (4.6). The equation $4\delta = \delta_2^2 \ln^2(24/\delta)$ governing δ is transcendental, but can be solved readily using an iterative procedure. The first iterate, starting with $\delta^{(0)} = \delta_2^2/4$, gives at once the leading-order expression $\delta = (\delta_2^2/4) \ln^2(96/\delta_2^2)[1 + o(1)]$. We note that in expressions of the form $\log(k/\delta)$, if k is $O(1)$ and $\delta \ll 1$, then $\log(k/\delta) = \log(1/\delta)[1 + o(1)]$, and for simplicity we always

take $k = 1$. The solution of (B 11) is then

$$\left. \begin{aligned} \delta &= \frac{\delta_2^2}{4} \ln^2(1/\delta_2^2)[1 + o(1)], & \delta_0 &= \frac{\delta_2}{\sqrt{2}} \ln(1/\delta_2^2)[1 + o(1)], \\ u_0 &= \ln(\sqrt{2} + \sqrt{3}) + O(\delta), & u_1 &= \frac{1}{\ln(1/\delta_2^2)}[1 + o(1)]. \end{aligned} \right\} \quad (\text{B } 12)$$

The values given by (B 12) are only accurate at very high values of $|F|$ due to the \ln terms. Therefore the values of δ_0 , u_1 , and δ taken in figure 8 have been obtained by numerical solution of the full matching conditions (B 6), (B 7), and (B 8) since the solution (B 12) is not sufficiently accurate even at the large value of $|F|$ considered.

Using the expressions of the Jacobian elliptic functions in terms of hyperbolic functions for $k \simeq 1$ from Abramowitz & Stegun (1972), the leading terms for G and G' are given by

$$G(X) = \begin{cases} X + 2\sqrt{3} - 3\sqrt{2} \tanh[\ln(\sqrt{2} + \sqrt{3}) + X/\sqrt{2}], & X = O(1) \\ X + 2\sqrt{3}, & X \gg 1, \end{cases} \quad (\text{B } 13)$$

$$G'(X) = 1 - 3/\cosh^2[\ln(\sqrt{2} + \sqrt{3}) + X/\sqrt{2}] \quad \forall X. \quad (\text{B } 14)$$

We will take as boundary layer width the distance between the matching point of the regular and asymptotic solution and the wall, which corresponds to the X value

$$X_{\text{match}} = [6/(r_3 - r_1)]^{1/2}(K + u_1 - u_0) = \frac{1}{\sqrt{2}} \ln \frac{1}{\epsilon}. \quad (\text{B } 15)$$

REFERENCES

- ABRAMOWITZ, M. & STEGUN, I. A. 1965 *Handbook of Mathematical Functions*. Dover.
- ALI, M. E. & WEIDMAN, P. D. 1993 On the linear stability of cellular spiral Couette flow. *Phys. Fluids A* **5**, 1188.
- BANKS, W. H. H. & ZATURSKA, M. B. 1992 On flow through a porous annular pipe. *Phys. Fluids A* **4**, 1131.
- BARENBLATT, G. I. 1996 *Scaling, Self-similarity and Intermediate Asymptotics*. Cambridge University Press.
- BENDER, C. M. & ORSZAG, S. A. 1978 *Advanced Mathematical Methods for Scientists and Engineers*. McGraw-Hill.
- BERMAN, A. S. 1953 Laminar flow in channels with porous walls. *J. Appl. Phys.* **24**, 1232.
- BERMAN, A. S. 1958 Laminar flow in an annulus with porous walls. *J. Appl. Phys.* **29**, 71.
- BRADY, J. F. 1984 Flow development in a porous channel and tube. *Phys. Fluids* **27**, 1061.
- BRADY, J. F. & ACRIVOS, A. 1981 Steady flow in a channel or tube with an accelerating surface velocity. An exact solution to the Navier–Stokes equations with reverse flow. *J. Fluid Mech.* **112**, 127.
- BURGERS, J. M. 1948 A mathematical model illustrating the theory of turbulence. *Adv. Appl. Mech.* **1**, 171.
- CANUTO, C., HUSSAINI, M. Y., QUARTERONI, A. & ZANG, T. A. 1987 *Spectral Methods in Fluid Dynamics*. Springer.
- CUNNING, G. M., WEIDMAN, P. D. & DAVIS, A. M. J. 1998 Radial stagnation flow on a rotating circular cylinder with uniform transpiration. *J. Engng Maths* **33**, 113.
- DURLOFSKY, L. & BRADY, J. F. 1984 The spatial stability of a class of similarity solutions. *Phys. Fluids* **27**, 1068.
- GILCHER, R. O. 1986 Plasmapheresis technology. *Vox. Sang.* **51** (Supplement 1), 35.
- GUCKENHEIMER, J. & HOLMES, P. 1986 *Nonlinear Oscillations, Dynamical Systems, and Bifurcations of Vector Fields*. Springer.
- HALLSTROM, B. & LOPEZ-LEIVA M. 1978 Description of a rotating ultrafiltration module. *Desalination* **24**, 273.

- HILDEBRANDT, J. R. & SAXTON, J. B. 1987 The use of Taylor vortices in protein processing to enhance membrane filtration performance. In *Bioprocess Engineering Colloquium* (ed. R. C. Dean & R. M. Nerem). ASME Book No. G00422, p. 93.
- JOHNSON, E. C. & LUEPTOW, R. M. 1997 Hydrodynamic stability of flow between rotating porous cylinders with radial and axial flow. *Phys. Fluids* **9**, 3687.
- JOSEPH, D. D. 1977 Global stability of spiral Couette–Poiseuille flows. In *Stability of Fluid Motions*, vols I and II. Springer Tracts in Natural Philosophy 27–28. Springer.
- KELLER, H. B. 1977 Numerical solution of bifurcation and nonlinear eigenvalue problems. In *Applications of Bifurcation Theory* (ed. P. H. Rabinowitz). Academic.
- KORTSARTS, Y., BRAILOWSKY, I., GUTMAN, S. & SIVASHINSKY, G.I. 1997 On the stability of stretched flames. *Combust. Theory Modelling* **1**, 143.
- LUDWIG, H. 1964 Experimentelle nachprüfung des Stabilitätstheorien für reibungsfreie Stromungen mit schraubenlinienförmigen Stromlinien. *Z. Flugwiss* **12**, 304.
- LUEPTOW, R. M. 1995 Fluid mechanics of a rotating filter separator. In *Advances in Filtration and Separation Technology* (ed. K.-J. Choi), vol. 9, p. 283. American Filtration and Separation Society.
- MIN, K. & LUEPTOW, R. M. 1994 Hydrodynamic stability of viscous flow between rotating porous cylinders with radial flow. *Phys. Fluids* **6**, 144.
- PROUDMAN, I. 1960 An example of steady laminar flow at large Reynolds number. *J. Fluid Mech.* **9**, 593.
- SAFFMAN, P. 1992 *Vortex Dynamics*, §13.3. Cambridge University Press.
- SCHLICHTING, H. 1968 *Boundary Layer Theory*. McGraw-Hill.
- SIMÓ, C. 1990 On the analytical and numerical approximation of invariant manifolds. In *Modern Methods in Celestial Mechanics* (ed. D. Benest & C. Froeschlé). Editions Frontières, Paris.
- TAGG, R. 1994 The Couette–Taylor Problem. *Nonlinear Sci. Today* **4**, 1.
- TAKEUCHI, D. I. & JANKOWSKI, D. F. 1981 A numerical and experimental investigation of the stability of spiral Poiseuille flow. *J. Fluid Mech.* **102**, 101.
- TERRILL, R. M. 1967 Flow through a porous annulus. *Appl. Sci. Res.* **17**, 204.
- TERRILL, R. M. & THOMAS, P. W. 1969 On laminar flow through a uniformly porous pipe. *Appl. Sci. Res.* **21**, 37.
- WANG, C.-Y. 1974 Axisymmetric stagnation flow on a cylinder. *Quart. Appl. Math.* **32**, 207.
- WEISSBERG, H. L. 1959 Laminar flow in the entrance region of a porous pipe. *Phys. Fluids* **2**, 510.
- YUAN, S. W. & FINKELSTEIN, A. B. 1956 Laminar pipe flow with injection and suction through a porous wall. *Trans. ASME* **78**, 719.
- ZATURSKA, M. B. & BANKS, W. H. H. 1995 Flow in a pipe driven by suction at an accelerating wall. *Acta Mech.* **110**, 111.